Mineralogy and Petrology
https://doi.org/10.1007/s00710-026-00998-6

RESEARCH

Triassic volcanism in the Afyon Zone (NW Türkiye): evidence from U–Pb zircon ages, Sr–Nd isotopes, and geochemistry of an enriched mantle source

Zafer Aslan[1] · M. Selman Aydoğan[1] · Y. Kağan Kadıoğlu[2] · Özcan Yiğit[3]

Received: 21 August 2025 / Accepted: 11 June 2026

Abstract
In the northwestern part of the Afyon Zone, along the northern margin of the Anatolide–Tauride Block, which is generally regarded as a fragment of northern Gondwana during the Late Paleozoic, Triassic metavolcanic rocks are extensively exposed. These rocks comprise felsic and basic types distinguished by mineralogical and geochemical variations. Zircon U-Pb dating of the felsic metavolcanics yields an age of 233.4 ± 2.1 Ma, indicating a Triassic magmatic episode. Metavolcanics have high potassium-shoshonitic and calc-alkaline characteristics. They are enriched in large-ion lithophile elements (LILE), and depleted in high-field-strength elements (HFSE). They also show enrichment in light rare earth elements (LREE) relative to heavy rare earth elements (HREE). The relative enrichment of low-field-strength elements (LFSE) over HFSE, along with average $(La/Lu)_N$ ratios of 3–25, reflects typical calc-alkaline volcanism. The geochemical trends suggest that assimilation and/or crustal contamination may have occurred during magma evolution. Furthermore, they are considered to be related to the island arc and resemble Tholeiitic-type mid-ocean ridge basalts. Isotope data supports an enriched mantle source. The initial $^{87}Sr/^{86}Sr$ isotope ratios are 0.711429–0.716276 in metadacite and 0.709275–0.714190 in metabasic. The $^{143}Nd/^{144}Nd$ isotope ratios vary from 0.512349 to 0.512369 in metadacite, and from 0.512463 to 0.512509 in metabasic. The geochemical and isotopic data suggest that the parental magmas were derived from an enriched mantle source metasomatized by subduction-related components beneath the Afyon Zone. The northward subduction of the Paleozoic Tethyan oceanic lithosphere under the southern margin of Laurasia during the Triassic is interpreted to have triggered a regionally rift-related regime along the northern margin of Gondwana. The Triassic metavolcanic rocks are interpreted to represent the earliest magmatic products associated with the Paleotethys Ocean crust, formed along the northern margin of Gondwana.

Keywords Afyon zone · Triassic metavolcanic rocks · North Gondwana · Northwestern Türkiye

Introduction

The paleogeographic and tectonic evolution of the eastern Mediterranean region is primarily controlled by the opening and subsequent closure of the Paleotethys and Neotethys oceans between the Early Paleozoic and Early Paleogene periods (Şengör and Yılmaz 1981; Okay et al. 2001; Akal et al. 2024). The main tectonic domains of Anatolia (Fig. 1a) comprise, from north to south, the Pontides, the Anatolide–Tauride Platform (ATP), and the Afro-Arabian Plate (Okay and Tüysüz 1999). In northern Anatolia, the Pontides include the Sakarya, Istanbul, Zonguldak, and Rhodope-Strandja zones, all of which were significantly affected by the Variscan orogenic events (Moix et al. 2008).

Editorial handling: M. Moazzen

✉ Zafer Aslan
zaslan@balikesir.edu.tr

[1] Department of Geological Engineering, Balıkesir University, Çağış Campus, Balıkesir 10145, Türkiye

[2] Department of Geological Engineering, Ankara University, Gölbaşı 50th Year Campus, 35th Street, Block 1/G, Ground Floor, Gölbaşı, Ankara 06830, Türkiye

[3] Department of Geological Engineering, Faculty of Engineering, Çanakkale 18 Mart University, Terzioğlu Campus, Çanakkale 17100, Türkiye

Published online: 26 June 2026

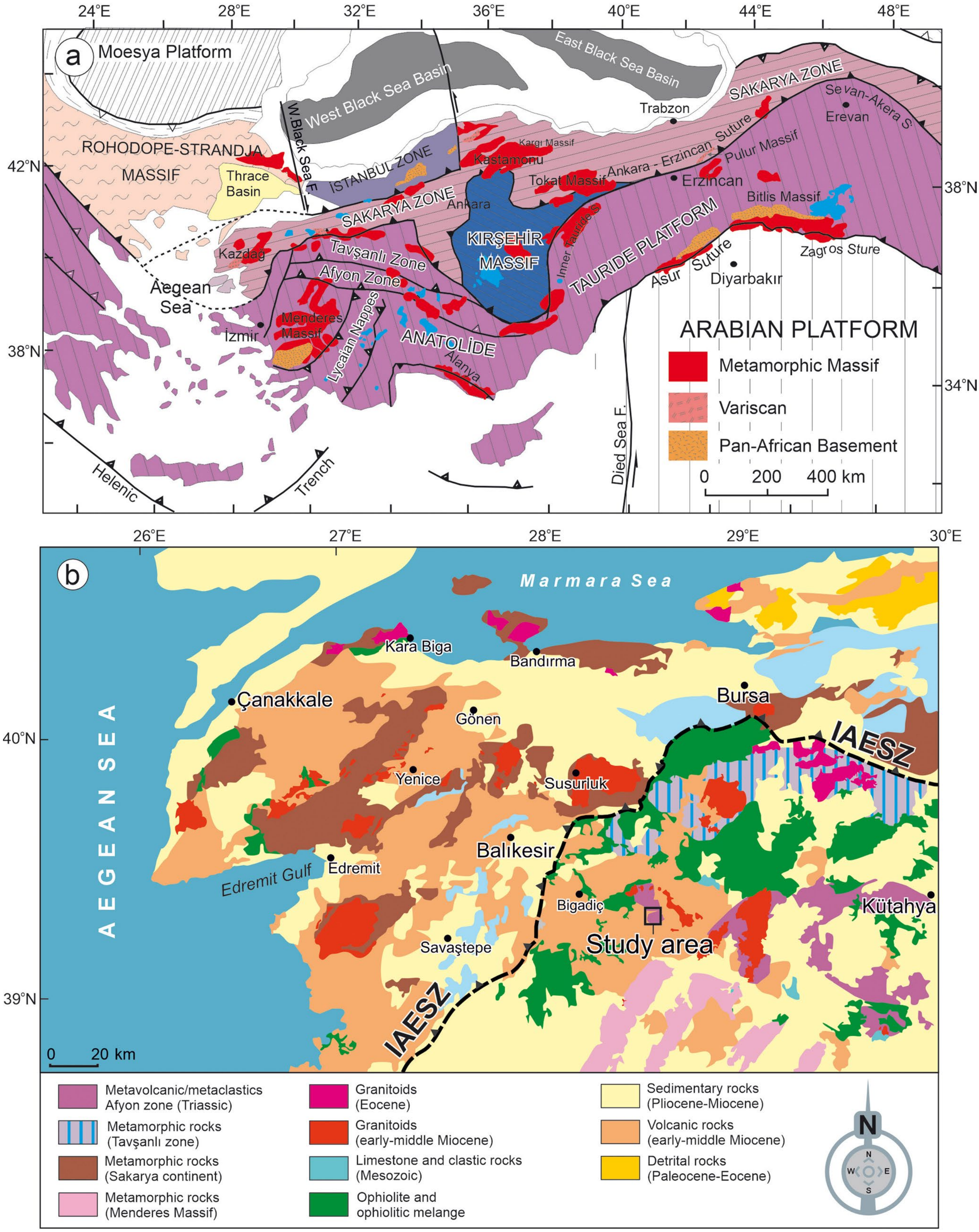

Fig. 1 (**a**) Major tectonic units and boundaries of Anatolia and adjacent regions (Okay and Tüysüz 1999); (**b**) Generalized geological map of the Biga Peninsula (modified after Pehlivan et al. 2007; Altunkaynak et al. 2012)

The east-west-trending İzmir-Ankara-Erzincan Suture Zone (IAESZ), extending for approximately 2000 km, represents one of the most important Neotethyan suture zones in Türkiye. It separates the Laurasian continental margin (Sakarya Continent and Rhodope-Pontide units) to the north from Gondwana-derived terranes of the Anatolide-Tauride Platform to the south (Şengör and Yılmaz 1981; Okay et al. 1996; Okay and Tüysüz 1999; Moix et al. 2008, 2011). The suture zone is mainly composed of discontinuous Mesozoic ophiolites and accretionary ophiolitic mélange complexes (Dilek and Thy 2006). These ophiolitic assemblages are interpreted as fragments of Tethyan oceanic lithosphere, representing oceanic basins that developed between Eurasia and Gondwana (Şengör and Yılmaz 1981; Robertson and Dixon 1984; Dilek and Moores 1990). Locally, the suture also contains well-preserved island-arc sequences (Göncüoğlu et al. 2006; Çelik et al. 2011) and extensive Mn-oxide deposits hosted by radiolarian chert blocks within the mélange complexes (Aydoğan 2021).

The ATP represents the easternmost continuation of the Apulian, forming a crucial segment of the southern passive continental margin of the Neo-Tethys Ocean. It is generally interpreted as a continental fragment that rifted from the northern margin of Gondwana during the Triassic, in response to the opening of the southern branch of the Netethys ocean (Şengör and Yılmaz 1981; Şengör et al. 1984; Pourteau et al. 2013; Akal et al. 2024). The ATP is composed of two principal tectonic belts: the Anatolides and the Taurides. Among these, the Tauride Belt consists predominantly of non-metamorphosed to very low-grade metamorphic sedimentary sequences ranging in age from the Early Paleozoic to the Early Cenozoic (Okay 1984). This belt represents the southern, relatively stable portion of the ATP and is regarded as a typical example of a Cimmerian continental block that rifted from the northern margin of Gondwana during the Triassic opening of the Neo-Tethys Ocean (Şengör 1979). It marks the rifting and opening of the Paleotethys Ocean to the north during the Devonian period and the Neotethys Ocean to the south during the Permian period (Moix et al. 2008). Its evolution is similar to that of the Cimmerian-Iranian blocks located to the east in Middle to Late Triassic time (Moix et al. 2008). It comprises a Precambrian basement, overlain by a Paleozoic-Mesozoic cover, which is mainly composed of carbonate platform-type sediments at the Beydağları area of southwestern Türkiye (Stampfli and Borel 2002; Stampfli et al. 2003). The Tauride belt exhibits no evidence of Variscan deformation (Şengör et al. 1984; Hetzel and Reischmann 1996; Dannat and Reischmann 1998). The Anatolide refers to the metamorphic Alpine tectonic unit that crop out along the northern margin of the ATP, and is considered to be the metamorphic equivalent of the Taurides and consist of tectono-metamorphic zones ranging the Late Cretaceous to the Eocene and running from north to south including the Tavşanlı Zone, the Afyon Zone and the Menderes Massif (Okay et al. 1998, 2001; Candan et al. 2005, 2016; Pourteau et al. 2013; Akal et al. 2024). Of these zones, Tavşanlı is characterised by Late Cretaceous blueschist metamorphism (Okay et al. 1998; Sherlock et al. 1999). It represents the northward subduction of the continental margin of the Anatolian platform. It has been thrust over the Afyon zone, which is composed of metamorphosed sedimentary rocks from the Devonian to Paleocene periods (Okay et al. 1996). These rocks are believed to have originated from the deeply buried northern margin of the Taurides during the closure of the northern branch of the Neotethys (Okay et al. 1998; Candan et al. 2005; Pourteau et al. 2013).

The Afyon Zone was first defined by Okay (1984), who reinterpreted the "low-grade metamorphic uppermost part of the Menderes Massif" described by Akdeniz and Konak (1979a, b) as well as the "low-grade metasedimentary rocks" identified by Kaya et al. (1995) as the deeply submerged, high pressure – low temperature (HP–LT) metamorphic part of the northern margin of the ATP. Güngör et al. (2025) stated that palaeontological evidence reveal that the upper part of the Afyon Zone succession (Budağan Limestone) dates to the Late Triassic to Kimmeridgian in age in the Emet region (western Türkiye) and reported as age of 237.4 ± 1.1 Ma for the metarhyolite in the Hasköy Formation (Akhisar region, western Türkiye).

Subsequently, based on lithostratigraphic and structural similarities, several researchers (e.g., Göncüoğlu et al. 1997; Özcan et al. 1988) proposed the term Kütahya-Bolkardağ Belt, redefining the region as a Paleozoic-Mesozoic metamorphosed sedimentary and carbonate sequence that represent the northern passive continental margin of the ATP. Within this belt, Göncüoğlu et al. (2003) recognized four main lithostratigraphic units: (i) a Silurian–Devonian carbonate succession, (ii) Carboniferous-Permian metaclastics and metavolcanics containing Carboniferous limestone blocks, (iii) Mesozoic clastic and carbonate sequences, tectonically overlain by Late Cretaceous ophiolitic nappes, and (iv) a Cenozoic sedimentary cover. This stratigraphic framework reflects the complex tectonometamorphic evolution of the northern margin of the ATP, recording stages of Paleozoic passive margin deposition, Mesozoic rifting, and Late Cretaceous-Eocene subduction–accretion processes along the northern branch of the Neotethys ocean.

Earlier pioneering studies have documented the presence of both acidic and basic magmatic rocks of Triassic age within the ATP. These include studies on magmatic rocks from the Menderes Massif (246 − 235 Ma; Koralay et al. 2001), the Karaburun Peninsula (247 − 239 Ma; Akal et al. 2011), and the Afyon Zone (245 − 229 Ma; Akal et al.

2012; Özdamar et al. 2013; Akal et al. 2024). Examining these Triassic magmatic rocks reveals extensive magmatic activity along the northern margin of Gondwana during the initial stages of Neotethyan rifting. Evidence from detrital zircon geochronology supports the existence of contemporaneous Triassic magmatism and sedimentation. Detrital zircon age populations from Triassic sedimentary successions in the Taurus Mountains (e.g., Ustaömer et al. 2020) and metasedimentary units of the Menderes Massif further record contributions from Triassic magmatic sources. These findings suggest that Triassic magmatism was regionally extensive, and that magmatic activity played a key role in the tectonomagmatic evolution of the ATP during the initial opening of the Neo-Tethys Ocean. Understanding the origin of these Triassic magmatic rocks is crucial for unravelling the tectonic evolution of the northern margin of Gondwana during the Late Paleozoic and Early Mesozoic periods.

Only a limited number of studies have adressed Triassic bimodal volcanism in the region. The present investigation offers a comprehensive reference framework for reconstructing the dynamic evolutionary history of the ATP through an integrated assessment of its Triassic magmatism, geochemical characteristics, and geodynamic setting.

Geological setting

Regionally, from north to south, the Tavşanlı Zone (Campanian, 80 ± 5 Ma), the Afyon Zone (approximately 70 Ma; Pourteau et al. 2013), and the Menderes Massif (Middle Eocene), represent metamorphosed fragments that were likely derived from the ATP. Within the regional tectonic framework, the HP–LT metamorphic assemblages of the Afyon Zone occupy an intermediate position between the Tavşanlı Zone and the Menderes Massif. The zone can be traced for roughly 750 km along a northwest-southeast trend, extending from Kütahya in the northwest through Afyon and Konya to the Bolkardağ (Niğde) region in the southeast. Stratigraphically, the Afyon Zone consists of a Pan-African metamorphic-plutonic basement, which is unconformably overlain by a Mesozoic cover sequence comprising metasedimentary and metavolcanic rocks. The basement reflects Barrovian-type amphibolite-facies metamorphism and comprises garnet-mica schists that are intruded by sodic amphibole-bearing metagabbros and leucocratic metagranites, indicating multiple magmatic-metamorphic episodes during its tectonothermal evolution (Candan et al. 2005, 2016; Akal et al. 2005, 2012, 2024). The metamorphic basement is unconformably overlain by a continuous metasedimentary sequence ranging in age from the Triassic to the early Palaeocene. This sequence begins with basal quartz metaconglomerates, passing upwards into phyllites, reflecting a gradual shift from proximal to more distal depositional environments during basin evolution (Candan et al. 2005). Regionally, Triassic (Scythian-Carnian) metaconglomerates form a prominent basal unit, reaching thicknesses of over 1 km, and record intense syn-rift sedimentation associated with the initial stages of Neotethyan basin formation. They accumulated on a subaerial continental surface influenced by normal faulting, forming alluvial fan complexes (Özcan et al. 1988; Göncüoğlu et al. 2003; Candan et al. 2005; Akal et al. 2005, 2012).

According to Pourteau et al. (2013), metamorphic rocks of the Afyon Zone are characterized by high-pressure/low-temperature metamorphism under blueschist facies conditions, dated to approximately 70 Ma, Late Cretaceous. The rock successions of zone are tectonically overlain by the blueschists of the Tavşanlı Zone. Candan et al. (2005) highlihted that Fe-Mg-carpholite-bearing quartz segregations imply temperatures of about 350 °C and minimum pressures of 6–9 kbar, corresponding to burial depths of about 30 km for the Mesozoic cover series and the underlying Pan-African basement. These rocks are unconformably overlain by Upper Palaeocene-Lower Eocene sedimentary rocks, indicating a Paleocene age for the regional HP – LT metamorphism (Candan et al. 2005). The ophiolitic units that migrated southward due to the closure of the Neotethys underwent burial metamorphism beneath the Tavşanlı Zone (Candan et al. 2005).

The Afyon Zone is made up mainly of a pre-Triassic metamorphic basement unconformably overlain by a Triassic to Upper Cretaceous (Campanian) metamorphic cover sequence, as established through paleontological and stratigraphic evidence (Özcan et al. 1988; Göncüoğlu et al. 2007). According to Candan et al. (2005), the central part of the Afyon Zone, extending across the Afyon and Konya regions and along the eastern and southeastern margins of the Menderes Massif, can be subdivided into two distinct lithostratigraphic assemblages: (1) a lower assemblage of comprising amphibolite-facies schists interlayered with mafic and felsic metavolcanic rocks, representing the metamorphic basement complex, and (2) an upper assemblage consisting of low-grade metasedimentary rocks, including metaconglomerate, schist, phyllite, and metacarbonate units, forming the metamorphic cover series (Akal et al. 2024; Güngör et al. 2025).

In the region (Fig. 1b), post-collisional granitic suites (Alaçam, Koyunoba, Eğrigöz, Baklan), which are well exposed in western to northwestern Türkiye, intruded the pre-Triassic basement rocks (Akal et al. 2007; Aslan et al. 2017, 2020a). The ignimbrites associated with the explosive and highly active volcanism in the region occur as remarkably thick sequences within and around the study area.

Analytical methods

A total of 72 samples from the study area, consisting of 41 metadacite samples and 31 metabasite samples were subjected to major- and trace-element analyses. The rock samples were crushed in a Retsch rock crusher and then ground in an automated Fritsch mortar grinder using a tungsten carbide mill. A 4-g sample was compressed with 0.9 g of binder material (wax) in a hydraulic press to form a press-pastille. Subsequently, geochemical analyses were performed using a Spectro X-Lab 2000 polarized energy dispersive X-ray fluorescence (PED-XRF) device equipped with a 400 W Rh end-window tube and Si(Li) detector, employing the Tq-7220 and GEO-7220 methods (for details see Kadıoğlu et al. 2006, 2009).

Additional major- and trace-element concentrations were determined using inductively coupled plasma-optical emission spectrometry (ICP-OES). For this, 0.2 g of powdered sample were fused with 1.5 g of $LiBO_2$, followed by dissolution in 100 ml of 5% HNO_3. Spectra were recorded by means of a Spectro Genesis ICP-OES system. Analytical accuracy and precision were monitored using STD OREAS30A (https://www.oreas.com/crm/oreas-30 A; accessed 8 June 2026), STD OREAS262 (https://www.oreas.com/crm/oreas-262; accessed 1 June 2026), STD SO-19 (see electronic supplementary material ESM2), STD GS311-1 (https://geostats.com.au/certs/GS311-1.pdf; accessed 4 June 2026) and STD GS910-4 (https://geostats.com.au/certs/GS910-4.pdf; accessed 4 June 2026).

The REE analyses were performed by means of inductively coupled plasma-mass spectrometry (ICP-MS), after complete digestion of a 0.25 g powdered aliquot in a mixture of four acids. Loss on ignition (LOI) was determined from the mass difference between pre- and post-combustion weights after heating the powdered samples to 1000 °C. The ICP-MS analyses were done by means of a Thermo Fischer Element 2 system, using and SDT SO 19 (ESM2) as analytical reference material.

U-Pb zircon age analysis was performed on a single metadacite sample. Zircon grains used in the U–Pb analysis were separated from metadacite sample using traditional magnetic separation and dense liquid techniques. Representative zircon grains were manually selected under a binocular microscope, mounted on epoxy resin disks, polished, and coated with a 50 nm thick gold film. Cathodoluminescence (CL) images were taken to reveal the internal textures of zircon crystals and select suitable points for analysis. U-Pb isotopic analyses of the zircon grains were performed using the secondary ion mass spectrometry (SIMS) technique, employing a SHRIMP II system manufactured by Australia Scientific Insturuments, following the analytical procedure described by Black et al. (2003a). The primary $(O_2)^-$ ion beam intensity ranged from 4 to 5 nA, and the spot size was approximately 30 µm. Each analytical site was rastered for 120–180 s prior to measurement. Five scans across the relevant mass stations were completed for each age determination. Zircon reference SL13 (Black et al. 2003b) was employed for elemental abundance determination and, TEMORA 1 (Black et al. 2003a) was used for $^{206}Pb/^{238}U$ calibration. Common Pb corrections were applied using measured ^{204}Pb values and assuming a Broken Hill Pb isotopic composition for common lead. SQUID 1.0 and ISOPLOT software (Ludwing 2003) were used for data reduction and analysis.

Sr and Nd isotope analyses were performed on a total of nine samples, including six metadacites and three metabasites. Samples were dissolved in a mixture of $HF+HClO_4$ in sealed Savillex beakers and heated on a hot plate for one week to ensure complete decomposition of the silicate matrix. After complete digestion, separation of Rb, Sr, and LREE was carried out using conventional cation-exchange chromatography. Sm and Nd fractions were subsequently further purified on a second cation-exchange column, which was carefully conditioned and eluted using dilute HCl to obtain high-purity REE fractions suitable for isotopic analysis. The analyses were performed using a VG Miromass VG354 multi-collector mass spectrometer. The $^{87}Sr/^{86}Sr$ and $^{146}Nd/^{144}Nd$ ratios were confirmed by mass separation as $^{87}Sr/^{86}Sr=0.1194$ and $^{146}Nd/^{144}Nd=0.7219$, respectively. The $^{87}Sr/^{86}Sr$ ratio was corrected according to the NBS-987 Sr = 0.710250 standard, and the $^{146}Nd/^{144}Nd$ ratio was corrected according to the La Jolla Nd = 0.511860 standard (Thirlwall 1991; Li et al. 2012). The uncertainties in results of concentration analyses due to isotopic dilution are 2% for Rb, 0.5% for Sr, 0.2% for Sm, and 0.5% for Nd. Detailed explanation of sample preparation, errors and analytical precision is provided in Zhang et al. (2002).

Results

Lithology and petrography

In the study area, the Afyon Zone consists of pre-Triassic metamorphic rocks and Triassic metavolcanic rocks, which are overlain in an unconformity (Fig. 2a-c). The pre-Triassic basement rocks generally comprise phyllite, schist and intercalated marble levels, as well as metaplutons. Basement of the Afyon Zone is composed predominantly of quartz-rich phyllite and quartz-sericite-muscovite schist, which locally contain marble lenses. The phyllites exhibit well-developed foliation, and are composed chiefly of sericite, chlorite, and quartz minerals. These metamorphic rocks are intruded by Carboniferous granite porphyry and

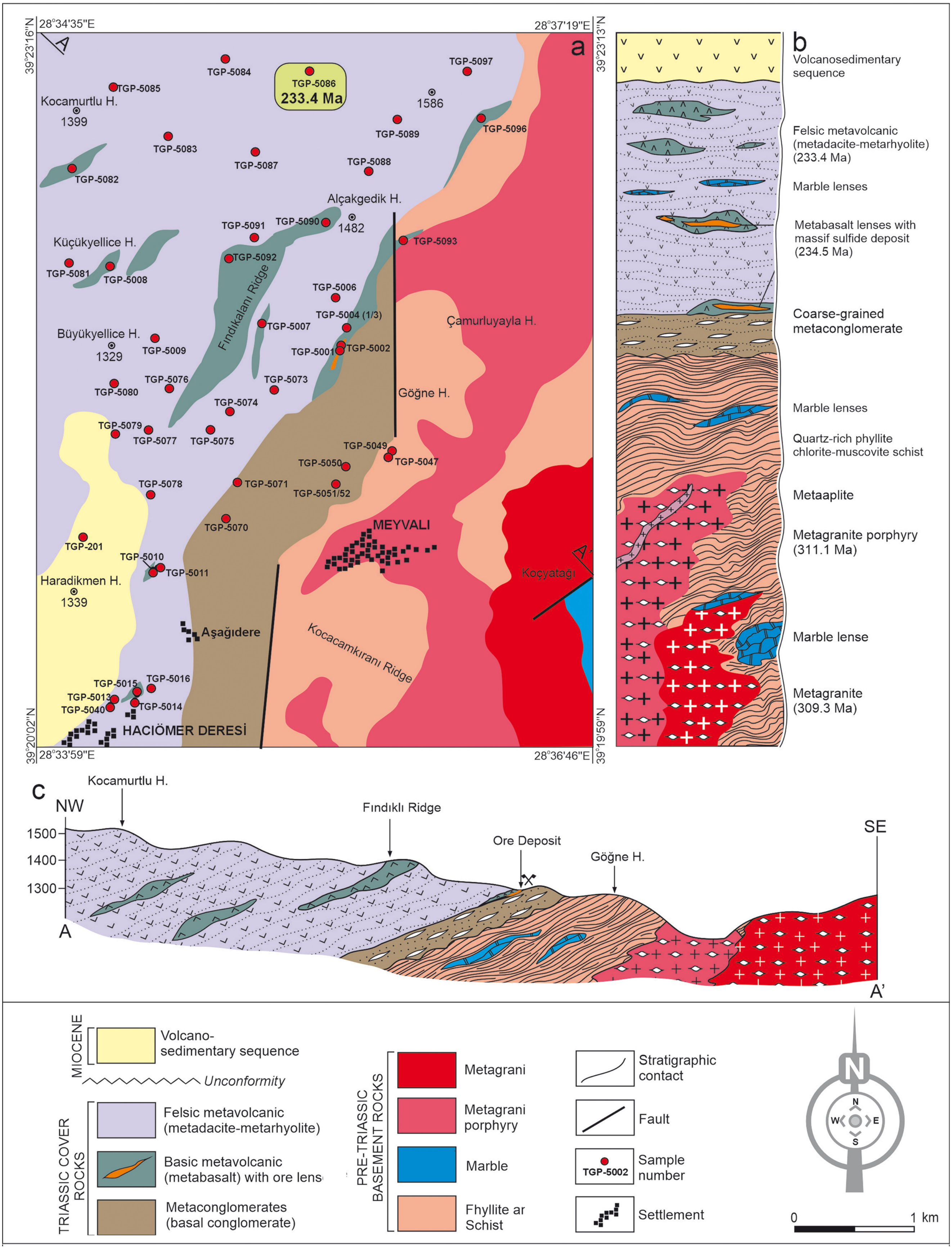

Fig. 2 Geological map of the study area (modified after Candan et al. 2016)

granite bodies (315 to 331 Ma), which are metamorphosed and represent the late Paleozoic magmatic activity in the region. (Fig. 2a-c). Overlying these basement rocks are coarse-grained metaconglomerate and metavolcanic rocks, referred to as the Triassic cover sequence (Akal et al. 2011). The quartz-rich metaconglomerates occur at the base of the basic metavolcanic rocks, directly above the phyllite, and generally contain felsic rock fragments along with coarse feldspar and quartz minerals (Fig. 3a, b). The metaconglomerate consists mainly of coarse quartz, K-feldspar, and muscovite, comprising coarse-grained, angular, and fragmented quartz clasts (Fig. 3c). These metaconglomerates are interpreted to record rifting and rapid uplift processes along the northern continental margin of Gondwana, associated with the opening of the northern branch of the Neotethys Ocean, following the southward subduction of the Paleotethys oceanic crust (Candan et al. 2005; Akal et al. 2011).

The Triassic cover unit consists of partially metamorphosed basic and felsic metavolcanics. Basic metavolcanics are associated with felsic metavolcanic rocks and occur as lenses in the field. The long axis of the lenses is more than 1 km, while the short axis is a few hundred meters. The basalt-characterized unit has massive structure (Fig. 3d, e). Petrographically, they are generally fine-grained and consists of plagioclase and pyroxene as the main minerals (Fig. 3f). Plagioclase mineral is transformed into sericite and epidote as a result of weathering, while pyroxene also shows uralitization. The groundmass is composed of plagioclase microlites and crystallites. Volcanic glass crystallized into epidote, muscovite, chlorite, sericite, and calcite minerals

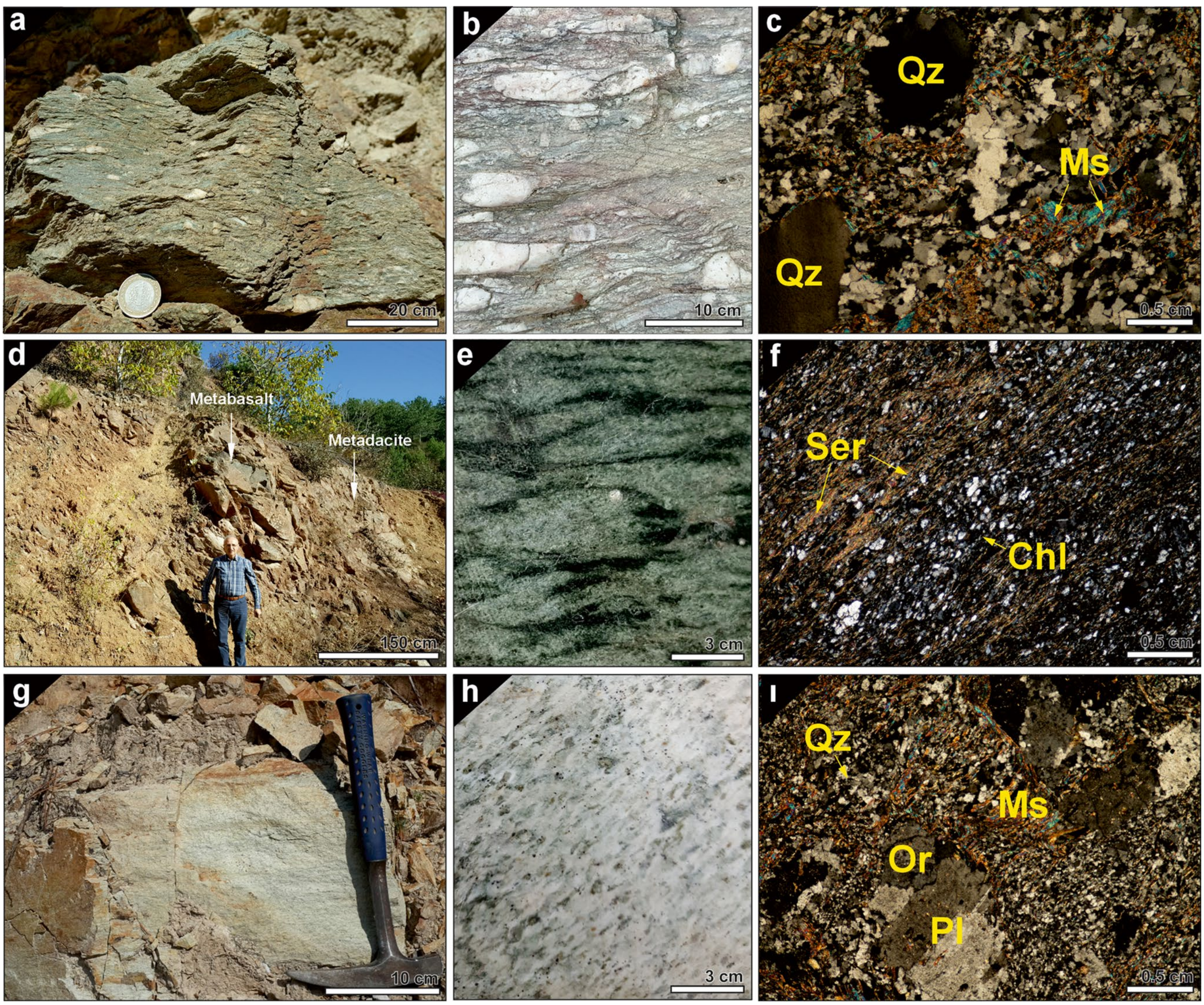

Fig. 3 Field photograph, hand specimen images, and cross-polarised transmitted-light photomicrographs illustrating the characteristic structures and textures of representative lithological units. (**a-c**) metaconglomerate; (**d-f**) metabasalt and (**g-l**) metadacite. *Chl* chlorite, *Ms* muscovite, *Or* orthoclase, *Pl* plagioclase, *Qz* quartz, *Ser* sericite

with a directional texture as a result of the metamorphism process. In addition, small amounts of rutile, ilmenite, and magnetite were observed. The massive sulfide mineralization found in the study area is distributed within lens-shaped metabasalt within Triassic-aged metavolcanic rocks. Importantly, this unit hosts massive sulfide deposits occurring as large lens-shaped bodies in the Gediktepe region. The Gediktepe massive sulfide mineralization is currently being mined within the study area (Aslan et al. 2020b). Felsic volcanic rocks in the region are generally observed as metadacite with subordinate metarhyolite in the study area(Fig. 3g, h). The main mineral content consists of quartz, plagioclase, and alkali feldspar (Fig. 3l), exhibiting a blastohypocrystalline texture, and has formed sericite and occasionally muscovite due to metamorphism.

U–Pb zircon age

One sample (TGP-5086; from a metadacitic rock) was subjected to SHRIMP U-Pb zircon dating. The results are provided in supplementary Table S1 in the electronic supplementary material (ESM1). A CL image, a Th/U versus age plot, a concordia diagram and a $^{206}Pb/^{238}U$ age plot presented in Fig. 4. The zircon grains are colorless and occur as short- to long-prismatic crystals, euhedral to subhedral (Fig. 4). The sizes of the zircon grains range from 50 to 150 µm. Oscillatory zoning was observed in most of the samples. Cathodoluminescence images reveal simple growth textures characterized by fine oscillatory and sector zoning, along with pyramidal terminations and oscillatory zoning in zircons, collectively indicating a magmatic origin

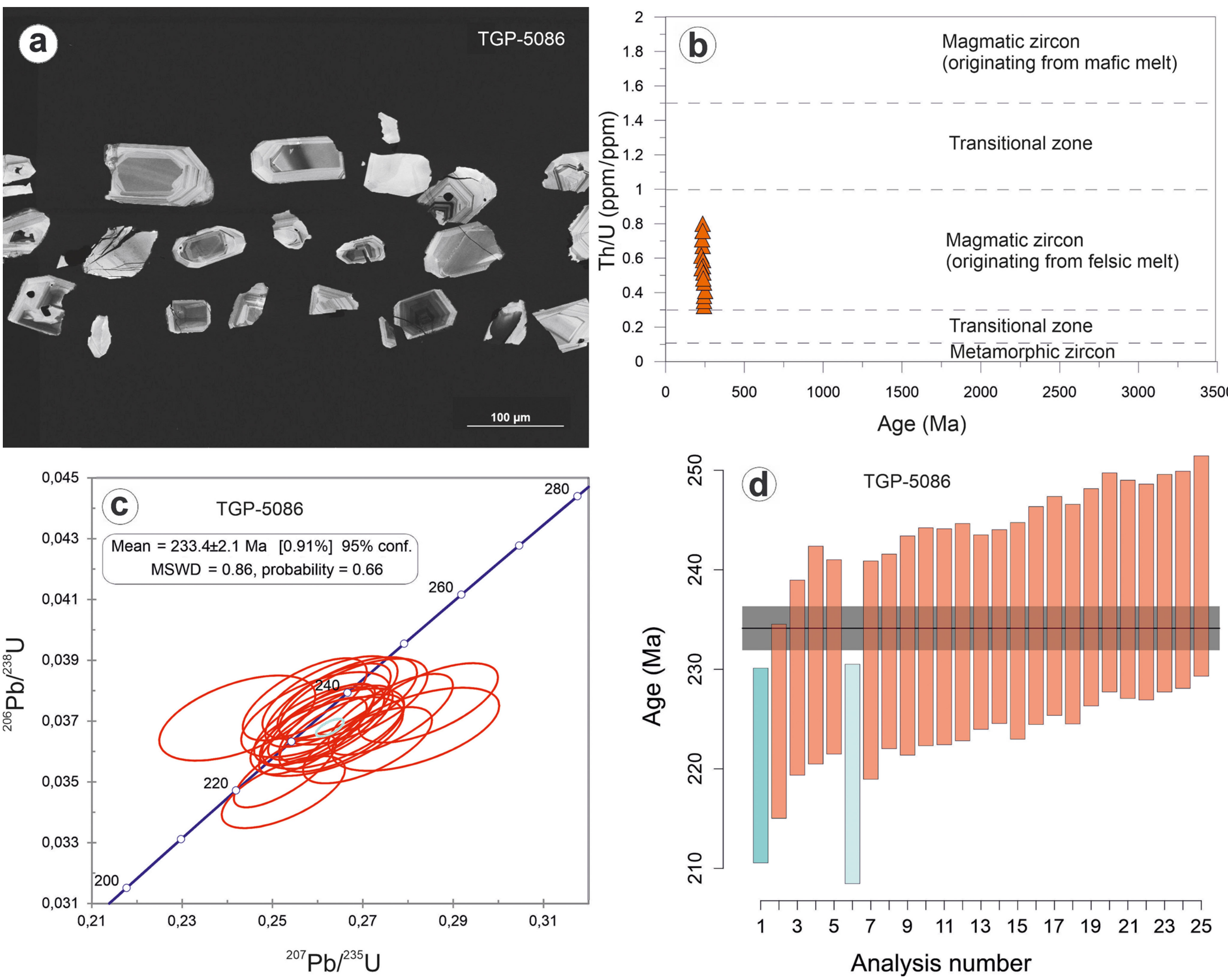

Fig. 4 (**a**) CL image of zircon crystals from the metadacite (TGP-5086) sample. (**b**) Th/U versus age plot, visualising that zircon crystals are magmatic in origin. (**c**) Concordia diagram visualising U-Pb isotopic results. The uncertainty of the mean age is quoted at the 95% confidence level (weighted by data point errors only; 0 fo 25 were rejected). (**d**) $^{206}Pb/^{238}U$ age plot

(Pupin 1980). Magmatic zircon is typically characterized by elevated Th/U ratios (>0.1), with values in this study ranging from 0.32 to 0.79 (see Aslan et al. 2020b). In contrast, metamorphic zircon generally exhibits lower concentrations of Th and U, along with Th/U ratios below 0.1 (Belousova et al. 2002; Kirkland et al. 2015). Moreover, all samples plot within the felsic-origin magmatic zircon field on the Th/U versus age diagram (see Fig. 4). The $^{206}Pb/^{238}U$ analysis results obtained from 25 points in sample TGP-5086 reveal that the rock is 233.4 ± 2.1 Ma old with a mean square weighted deviation (MSWD) of = 0.86 (see Fig. 4).

The obtained U-Pb zircon age is consistent with those previously reported for the metagranite and metagranite porphyry units in the region (Candan et al. 2016), although no prior U-Pb zircon data have been available for metadacitic rocks before this study. Because of the combined effects of metamorphism and ore-related alteration, direct age determination from the metabasic rocks was not feasible. The age of massive pyrite occurring within lenses hosted by the metabasic rocks was determined by the Re-Os isotopic method, yielding an age of 258.2 ± 5.2 Ma (Aslan et al. 2020b). This result implies that the formation of metabasic rocks likely occurred within a comparable Triassic period, consistent with the Late Triassic magmatic event recorded in the metadacitic rocks.

Whole-rock geochemistry

Geochemical analyses have been conducted on samples taken from Triassic-aged cover rocks that formed under low-grade regional metamorphism in and around Hacıömerderesi Village. Some of the samples with TGP numbers were subjected to REE analysis. Samples with codes beginning 44,962 represent rock samples located immediately below or above the ore. The main, trace and rare earth element analyses of the studied rocks are presented in Table S2 in ESM1 (analysis results taken from Aslan et al. 2020b).

In samples belonging to metadacite, SiO_2 varies in the range 62–78 wt%, K_2O in the range 0.45–6.89 wt%, Fe_2O_3 in the range 0.51–8.44 wt% and Na_2O in the range 1.07–5.01 wt%. In metabasic rocks, the values are SiO_2 between 44 and 58 wt%, K_2O between 0.01 and 5.22 wt%, Fe_2O_3 between 9.15 and 23.80 wt% and Na_2O between 0.01 and 4.72 wt% (Table S2). In metabasic samples located immediately above the ore body, these values are SiO_2 42 to 70 wt%, K_2O 0.60 to 5.36 wt%, Fe_2O_3 1.85 to 14.92 wt% and Na_2O 0.03 to 7.05 wt%. Although the K_2O value in metabasic rocks ranges from 0.01 wt% to 5.22 wt%, the average value is below 1 wt%. K_2O values are low in metabasalt, while Fe_2O_3 values are higher compared to metadacite. The analysis results show a wide range in both rock types. These differences, particularly in K_2O and Na_2O values, may be due to alteration. This situation may be caused by the Triassic-aged rocks undergoing both surface alteration and hydrothermal alteration due to magmatic activity in the region.

Metadacitic rock samples are located in the rhyolite and dacite fields in the total alkali-silica (TAS) diagram of Middlemost (1994; Fig. 5a). Metabasalt samples, on the other hand, are generally concentrated in the basalt and basaltic andesite areas. Some samples are located in the picrobasalts, trachybasalts, andesites, and even dacites regions. These differently distributed samples are metabasic rock samples immediately above and below the ore in the drilling logs and have been significantly affected by mineralization. This is particularly evident in mobile elements such as potassium and sodium. In the same diagram, all samples are located in the subalkaline region. In the Zr/TiO_2 versus Nb/Y diagram (Winchester and Floyd 1977), where effects such as contamination and alteration are not observed and some relatively immobile trace elements are considered, felsic metavolcanics generally occur in the rhyolite/dacite zone, while mafic metavolcanic rocks occur in the basalt and andesite/basalt zones (Fig. 5b). According to directional evaluations made in the alkali–iron–magnesium (AFM) triangle diagram (Irvine and Baragar 1971), felsic metavolcanic rocks are located in the calc-alkaline field, while some basic metavolcanic rocks plot in the tholeiitic field (Fig. 5c). Upon examining Table S2, it is understood that the FeO ratios in these rocks are quite high and that the samples show a directional trend toward the F corner of the AFM triangle. Additionally, the studied samples were evaluated in the Co-Th diagram, with metadacitic samples concentrated in the high potassium and shoshonitic field, while metabasic samples are concentrated in the calc-alkaline field (Fig. 5d).

Examining the changes in the main oxide components of metavolcanic rocks as the SiO_2 content increases reveals that the distribution of these components is either regular or irregular. The positive or negative trends observed in the main and trace elements in relation to SiO_2 content indicate magmatic crystal fractionation processes. Negative trends are present in TiO_2, Na_2O, Al_2O_3, Fe_2O_3, CaO, MnO, MgO, P_2O_5, and Sr, while positive trends are observed in K_2O, Rb, Zr, Nb, and Th (Fig. 6). Elements such as Ba exhibit irregular distributions. Changes in the Na_2O, Al_2O_3, CaO diagram relative to SiO_2 have particularly influenced the crystallization of plagioclases. The relationship between MgO and SiO_2 indicates the differentiation of the mafic mineral phase, particularly hornblende, while the variation diagram of Fe_2O_3 against SiO_2 suggests that Fe-Ti oxides and hornblende may be effective in crystallization (Gill 1981; Thirlwall et al. 1994). Similarly, the decrease in P_2O_5 and TiO_2 with increasing SiO_2 is associated with the crystallization of apatite and titanomagnetite minerals, respectively.

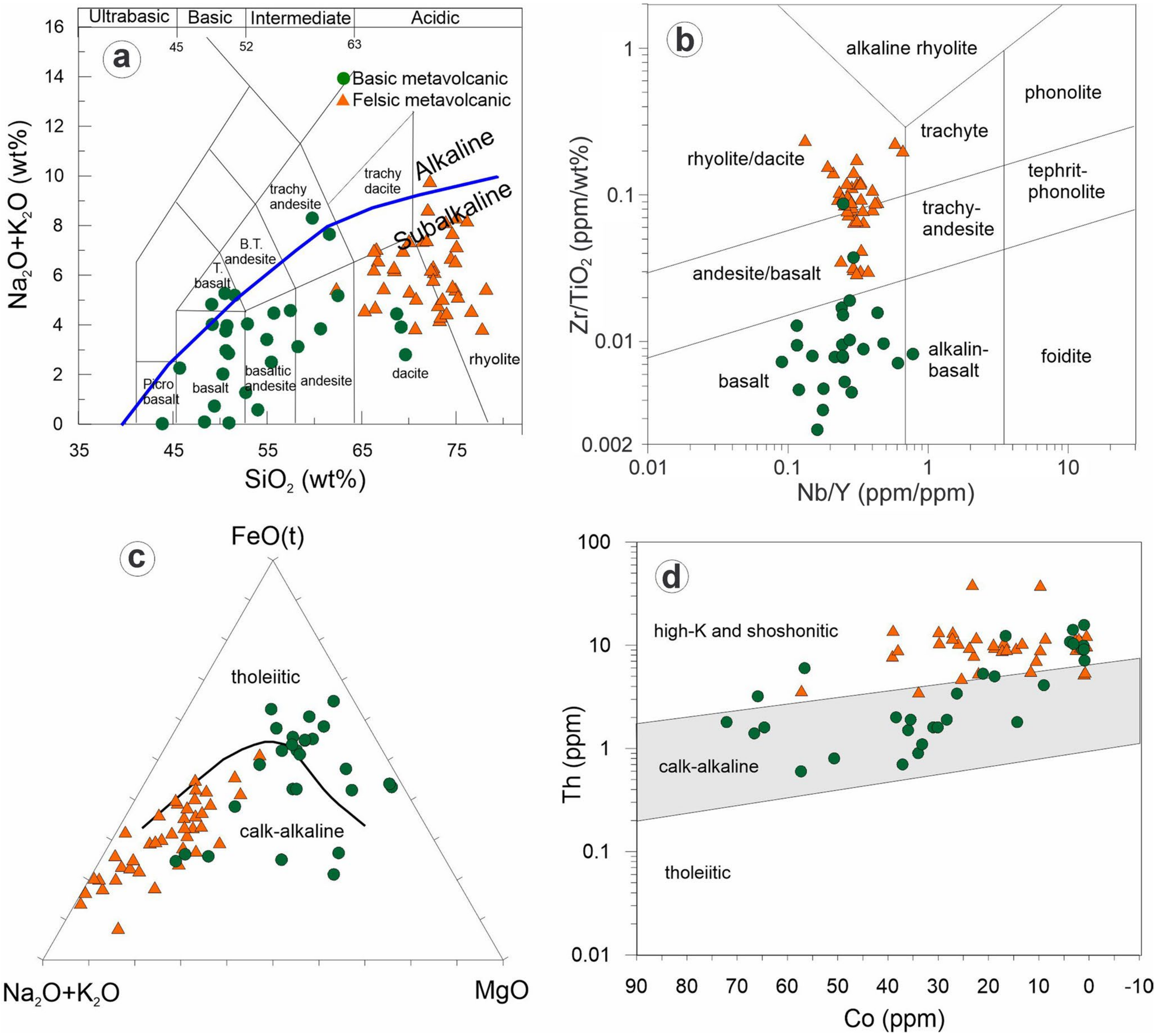

Fig. 5 (**a**) Na_2O+K_2O versus SiO_2 diagram of basic rocks (Middlemost 1994; alkali-subalkali boundary line according to Miyashiro 1978). (**b**) Zr/TiO_2 versus Nb/Y diagram. (**c**) Major oxides plotted in the alkali–iron–magnesium (AFM) diagram. The tholeitic-alkaline curve is from Irvine and Baragar 1971. FeO(t) – total Fe oxide, assuming all Fe to be ferrous. (**d**) Th versus Co plot (after Le Maitre et al. 2002). Symbols as in Fig. 5a are used in all plots

The change observed in Sr, an incompatible element, may be related to the crystallization of plagioclase. These findings reveal that the differentiation of plagioclase and hornblende minerals plays an important role in the development of metavolcanic rocks.

Although trace element distribution patterns in metadacite and metabasic samples show similar trends, more pronounced variations are observed in the concentrations of mobile elements in metabasic rocks. This is an indication of the change caused by mineralization in the rock. In trace element distribution diagrams normalized to the Normal mid-ocean ridge basalt (N-MORB) (Sun and McDonough 1989; Fig. 7a, b), metadacite and metabasic samples are enriched in LILE (e.g., Ba, Rb, U, Th) and, conversely, significantly depleted in HFSE. A notable Nb anomaly is present in both rock groups, which is thought to indicate the differentiation of apatite and Fe-Ti oxide minerals. In the distributions, Sr and Co values are logarithmically very low, while W and Cs values are very high. Co values are lower in samples close to the ore. The high W value is likely due to the samples being pulverized in a tungsten-carbide mortar. According to chondrite (Sun and McDonough 1989), in normalized rare earth element distributions (Fig. 7c, d), the trends of the samples are generally parallel, with enrichment in LREE and less

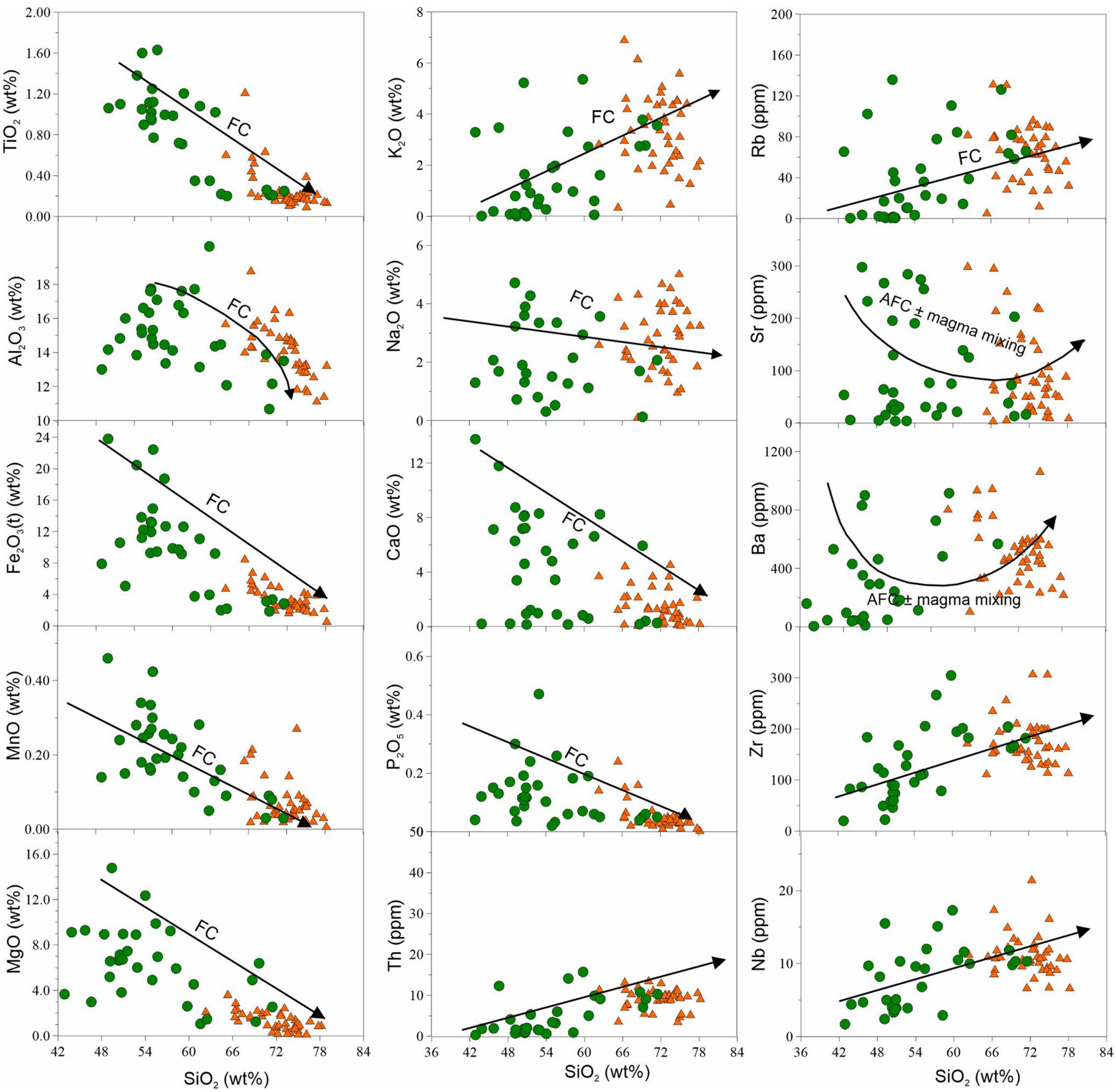

Fig. 6 Variation diagrams of major oxides and some trace elements relative to SiO_2 in metavolcanic rocks. AFC – assimilation and fractional crystallization; FC – fractional crystallization. Symbols as in Fig. 5

enrichment in HREE. Additionally, the rare earth element values of metabasic samples are higher than those of metadacitic samples. In metadacitic samples, $(La/Lu)_N$ values range from 2.42 to 25.45, and $(La/Sm)_N$ values range from 2.79 to 5.43, while in metabasic samples, $(La/Lu)_N$ values range from 1.84 to 10.84 and $(La/Sm)_N$ values range from 1.66 to 7.17, with average $(La/Lu)_N$ values of 20–25, hence exhibiting a moderately enriched and concave-shaped distribution. While a slight enrichment of rare earth elements is observed compared to chondrites, the concave-shaped rare earth element distributions in the samples indicate the differentiation of hornblende and plagioclase minerals (Thompson et al. 1984). Eu shows a very slight anomaly, with Eu_N values ranging from 0.31 to 1.00 in metadacites and from 0.32 to 1.32 in metabasic. This indicates the differentiation of plagioclase and K-feldspar (White and Patchett 1984; Bradshaw and Smith 1994; Smith et al. 1999; Elburg et al. 2002). The enrichment of LFSE elements over HFSE elements in rare earth elements and the average $(La/Lu)_N$ values in the range of 3–25 emphasize typical calc-alkaline volcanism.

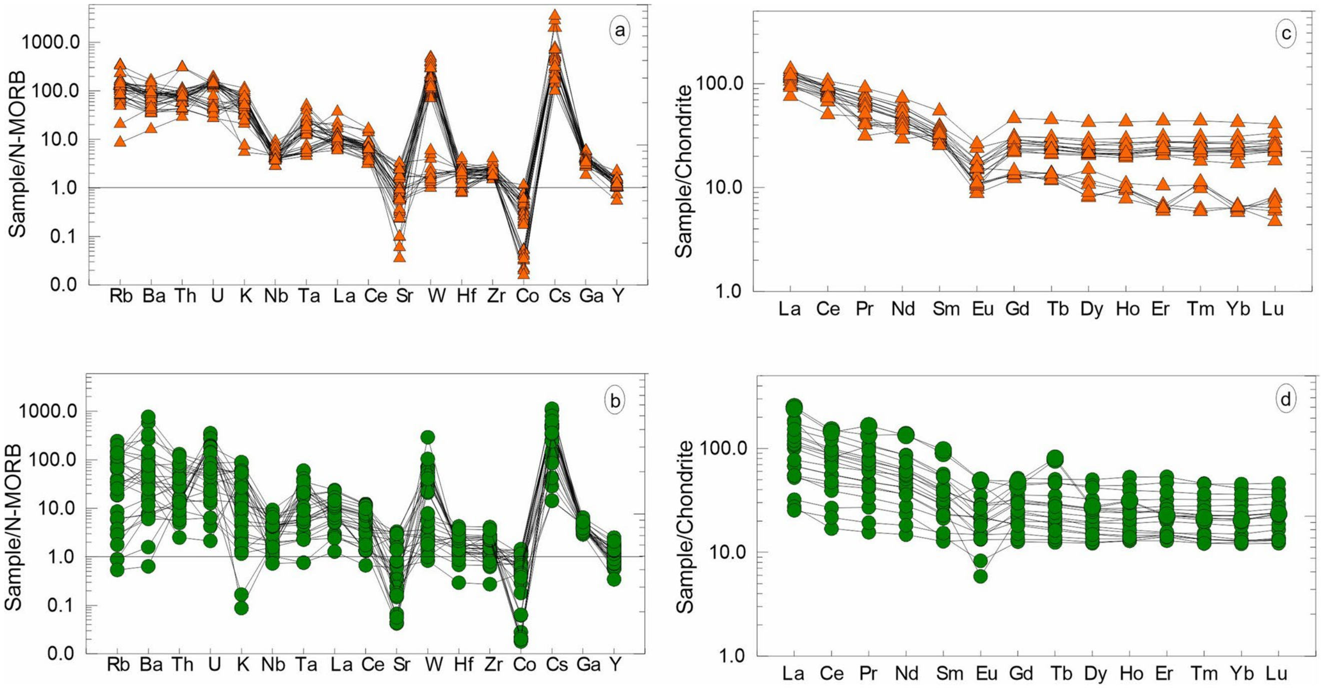

Fig. 7 Trace element distribution diagram of (**a**, **c**) metabasic and (**b**, **d**) metadacite rock samples normalised to normal mif-ocean ridge basalt (N-MORB; **a**, **b**) and chondrite (**c**, **d**). Chondrite values from Sun and McDonough (1989). Symbols as in Fig. 5

Sr and Nd isotopes

Isotope geochemistry explains the source and properties of magma in magmatic rocks, as well as their formation location and geodynamic status. Additionally, isotope data can be used to draw conclusions about events such as the mixing of different magmatic sources or the contamination of sources (Faure 2001). Since it is difficult to measure isotope values analytically with high precision, stable isotopes that do not undergo decay are used as references, and measurements are made using isotope ratios. Thus, the isotope amount is expressed as the ratio of the element's radiogenic isotope to its stable isotope. The values measured in laboratories are current isotope values, and the isotope ratios at the time of rock formation are used. For this purpose, age correction has been applied to the values (Jacobsen and Wasserburg 1980).

Using the mineralogical, petrographic, and geochemical properties of the rocks under investigation, fresh samples unaffected by surface and hydrothermal weathering were selected for Sr-Nd isotope analysis. Rb-Sr and Nd-Sm isotope analyses were performed on a total of 9 samples, including 5 metadacites and 4 metabasic, from the studied volcanic rocks. The analysis results are presented in Table 1 (obtained from Aslan et al. 2020b).

The initial $^{87}Sr/^{86}Sr$ and $^{143}Nd/^{144}Nd$ ratios, as well as the ƐNd(i) values, were calculated for the samples based on U-Pb SHRIMP zircon ages. The initial $^{87}Sr/^{86}Sr$ isotope ratios range from 0.709275 to 0.714190 in the metadacite, and from 0.711598 to 0.716276 in the metabasic. The $^{143}Nd/^{144}Nd$ isotope ratios range from 0.512391 to 0.512509 in the metadacite, and from 0.512349 to 0.512369 in the metabasic. Additionally, the ƐNd(i) values and Nd Model ages (TDM) range from −2.5 to −4.8 and 1.50 to 2.27 in the metadacite and from −5.2 to −5.7 and 1.32 to 1.71 in the metabasic (Table 1). The values for volcanic rocks are not continental, but rather indicate enriched mantle values. In the $^{87}Sr/^{86}Sr$ (i) versus εNd(i) diagram (Fig. 8), the samples generally lie outside the mantle line, showing a parallel orientation. When Early-Middle Miocene calc-alkaline lava samples from northwestern Anatolia are compared to metavolcanic rocks that have been examined, a similar $^{143}Nd/^{144}Nd$ ratio is shown, but a higher $^{87}Sr/^{86}Sr$ ratio is revealed (Fig. 8). When the data obtained in the study area are compared with regional data, a high $^{87}Sr/^{86}Sr$ ratio and a low $^{143}Nd/^{144}Nd$ ratio are observed. Evaluating the samples from the studied rocks on the $^{143}Nd/^{144}Nd$ diagram against $^{87}Sr/^{86}Sr$ shows that all samples deviate from the mantle interval and tend towards EMII (enriched mantle) (Fig. 8). The high $^{87}Sr/^{86}Sr$ and low $^{143}Nd/^{144}Nd$ ratios of the rock samples are consistent with an enriched continental lithospheric mantle (Altunkaynak et al. 2012).

Table 1 Results of Rb-Sr and Nd-Sm isotopic analyses of metavolcanic rocks

Sample	Rb (ppm)	Sr (ppm)	$^{87}Rb/^{86}Sr$	$^{87}Sr/^{86}Sr$	ISr (230 Ma)	Sm (ppm)	Nd (ppm)	^{144}Nd	^{144}Nd	f Sm/Nd	eNd(0)	eNd(T) 230 Ma	TDM(Ga)
TGP-5006	69.7	139.6	1.4479	0.714232	0.70950	5.07	24.3	0.1261	0.512369	−0.36	−5.2	−3.2	1.36
TGP-5080	95.6	79.3	3.4961	0.714381	0.70294	5	13.7	0.2206	0.512353	0.12	−5.6	−6.3	1.71
TGP-5083	70	53.5	3.7944	0.716276	0.70386	4.25	20.9	0.1229	0.512361	−0.38	−5.4	−3.2	1.32
TGP-5086	81.3	297.8	0.7917	0.711598	0.70901	5.97	29	0.1244	0.512349	−0.37	−5.6	−3.5	1.37
TGP-5087	130.5	5.4	70.0833	0.715479	0.48621	5.78	27.2	0.1285	0.512361	−0.35	−5.4	−3.4	1.41
TGP-5010	1.6	64.3	0.0722	0.71419	0.71395	1.95	6.9	0.1708	0.512509	−0.13	−2.5	−1.8	2.27
TGP-5015	1	36	0.0806	0.709275	0.70901	2.34	8.5	0.1664	0.512501	−0.15	−2.7	−1.8	2.08
TGP-5082	46.4	49.7	2.7074	0.711429	0.70257	4.18	17.2	0.1469	0.512391	−0.25	−4.8	−3.4	1.73
TGP-5090	22.6	30.7	2.1349	0.711933	0.70495	14.82	62.28	0.1438	0.512463	−0.27	−3.4	−1.9	1.50

eNd = [($^{143}Nd/^{144}Nd$)sample/($^{143}Nd/^{144}Nd$)CHUR − 1] · 10,000; f Sm/Nd = ($^{147}Sm/^{144}Nd$)sample/($^{147}Sm/^{144}Nd$)CHUR − 1; with ($^{143}Nd/^{144}Nd$)CHUR = 0.512638 and ($^{147}Sm/^{144}Nd$)CHUR = 0.1967

The model ages (TDM) were calculated using a linear isotopic ratio growth equation: TDM = 1/l · ln[1+($^{143}Nd/^{144}Nd$)sample − 0.51315)/($^{147}Sm/^{144}Nd$)sample − 0.2137]

Discussion

Fractional crystallization and assimilation

The major and trace element variations in the studied metavolcanic rocks display both positive and negative correlations with SiO_2, reflecting the effects of crystal fractionation. Accordingly, in Harker diagrams (Fig. 8), changes in Na_2O, Al_2O_3, and CaO values against SiO_2 indicate plagioclase, while the relationship between MgO and SiO_2 indicates amphibole and biotite, and changes in Fe_2O_3 against SiO_2 indicate Fe-Ti oxides and amphibole crystallization. The variation in the incompatible element Y may be related to amphibole crystallization, while the variation in Sr may be related to plagioclase crystallization. Additionally, the negative correlation between P_2O_5 and TiO_2 with SiO_2 is associated with the crystallization of apatite and titanomagnetite, respectively. The presence of a negative Eu anomaly further supports the role of feldspar fractionation. Specifically, plagioclase fractionation produces negative Sr and Eu anomaly values, while K-feldspar fractionation produces negative Ba and Eu anomalies. Overall, these geochemical relationships indicate that fractional crystallization of plagioclase, amphibole, and biotite played a dominant role in the evolution and differentiation of the studied metavolcanic rocks (Gill 1981; Thirlwall et al. 1994).

In the Zr-La diagram, metavolcanic rocks show a positive trend, indicating that they crystallized through mineral differentiation of the magma (Fig. 9a), while in the Sr diagram against MgO (Fig. 9b), an inverse relationship is observed, indicating plagioclase differentiation. Increasing Nb and Y changes against Zr (Fig. 9c, d) indicate plagioclase and hornblende differentiation. These geochemical relationships demonstrate that the metavolcanic rocks were primarily formed through a fractional crystallization process, with pyroxene, hornblende, and plagioclase playing dominant roles in magma differentiation. Additionally, binary diagrams were used to investigate assimilation and/or magma mixing events in the metavolcanic rocks. The Th–Th/Sm and Sr–Sr/Y diagrams (Fig. 9e, f) show a positive trend, indicating that assimilation and/or contamination were effective in the magma that formed the metavolcanic rocks.

Magma sources of metavolcanic rocks

The studied metavolcanic rocks were evaluated to determine whether they originated from a heterogeneous mantle source, reflect different degrees of partial melting of a common source, or evolved through mineral differentiation, magma mixing, and assimilation processes. The rocks display volcanic-arc geochemical signatures, with Ba/La

Fig. 8 Plot of (^{143}Nd/^{144}Nd) i versus (^{87}Sr/^{86}Sr)i. MORB compositions are from Zindler and Hart (1986) and the BSE composition from Hart et al. (1986). EMI and EMII – enriched mantle I and II; HIMU – mantle with high ^{238}U/^{204}Pb ratio; BSE – bulk silicate Earth; N-MORB – normal mid-ocean ridge basalt; E-MORB – enriched-mid-ocean ridge basalt. Symbols as in Fig. 5

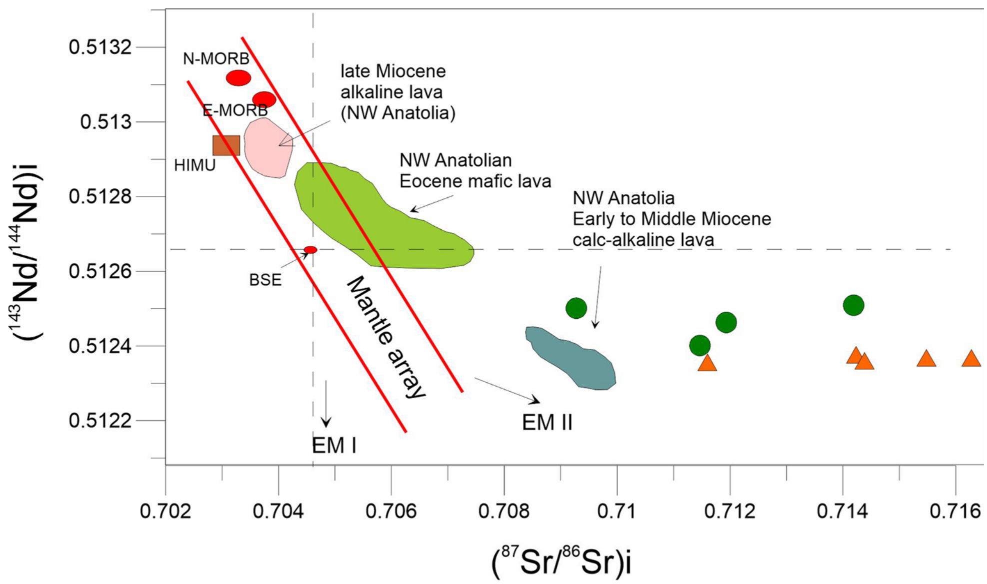

ratios ranging from 7 to 32 in metadacites and 2 to 130 in metabasalts. The wider range in the metabasalts is attributed to sample variability, particularly those collected from the immediate lower and upper sections of the ore-bearing zones. Elemental ratios such as Ba/Nb, La/Nb, Ba/La, Sm/Nd, and Nb/Th suggest a calc-alkaline affinity, consistent with subduction-related magmatism (Thompson et al. 1984; White and Patchett 1984; Bradshaw and Smith 1994; Smith et al. 1999; Elburg et al. 2002). The Zr/Y ratios range from 2.5 to 7.4 (average 4–5) in metadacites and 0.8 to 5.5 (average 2–3) in metabasalts, whereas Zr/Nb ratios vary from 9 to 38 (average 14–16) in metadacites and 4 to 32 (average 14–16) in metabasalts. These geochemical parameters indicate that the metavolcanic rocks were derived from partial melting of an enriched lithospheric mantle source, followed by fractional crystallization and limited crustal contamination during magmatic evolution.

In the Nb_N/Zr_N versus Zr diagram (Fig. 10a), used to determine the tectonomagmatic origin of the metavolcanic rocks, most samples plot within the field of collision-related calc-alkaline volcanic rocks. A few samples that fall outside this field correspond to those collected from the immediate footwall and hanging wall of the mineralization zone, reflecting localized geochemical modification. The Th/Yb versus Ta/Yb diagram (Fig. 10b), which discriminates between mantle sources and identifies possible crustal contamination or subduction-related enrichment, indicates that the analyzed samples were derived from magmas that evolved through fractional crystallization (FC) and display evidence of enrichment in loss-related components. Similarly, on the Ba/Nb–La/Nb diagram (Fig. 10c), all metavolcanic samples fall within the volcanic-arc field, consistent with subduction-related magmatism. In the Nb/La versus La/Yb diagram (Fig. 10d), most samples plot within the lithospheric mantle domain, while those collected near the mineralization zones fall close to the lithospheric–asthenospheric mantle mixing field, suggesting partial contribution from a deeper asthenospheric source. The La/Yb versus Th/Yb diagram (Fig. 10e) further supports an island-arc affinity for these metavolcanic rocks. The observed enrichment of LILE such as K, Ba, and Rb, relative to HFSE such as Nb and Ti, can be attributed to subduction-related fluid addition, crustal contamination, and/or crystal fractionation. Moreover, the vertical trend of the samples in the Rb/Y versus Nb/Y diagram (Fig. 10f) reinforces the interpretation that the magmas were affected by subduction-derived enrichment and/or crustal assimilation during their evolution.

Geodynamic applications

The Anatolide–Tauride Block is interpreted as part of Gondwana's northern passive margin during the Paleozoic (Cocks and Torsvik 2002; Okay et al. 2006; Okay and Nikishin 2015). Triassic magmatic events are attributed to the northward subduction of the Paleo-Tethys along the southern margin of the Laurasia (Reischmann et al. 2001; Mposkos and Krohe 2004; Anders et al. 2006; Zlatkin et al. 2017). Triassic magmatism is recorded across tectonic domains in Türkiye with Middle–Late Triassic activity. In the Late Permian-Triassic, the progressive consumption of the Paleo-Tethys Ocean, accompanied by the initiation of Cimmerian rifting and northward drift of Cimmerian continental fragments, led to the progressive detachment of these passive-margin segments from Gondwana and ultimately to the opening of Neotethyan oceanic basins (Stampfli and Borel 2002; Stampfli et al. 2003; Domeier and Torsvik 2014). This large-scale geodynamic reorganization resulted in the subsequent dispersal of these blocks into different

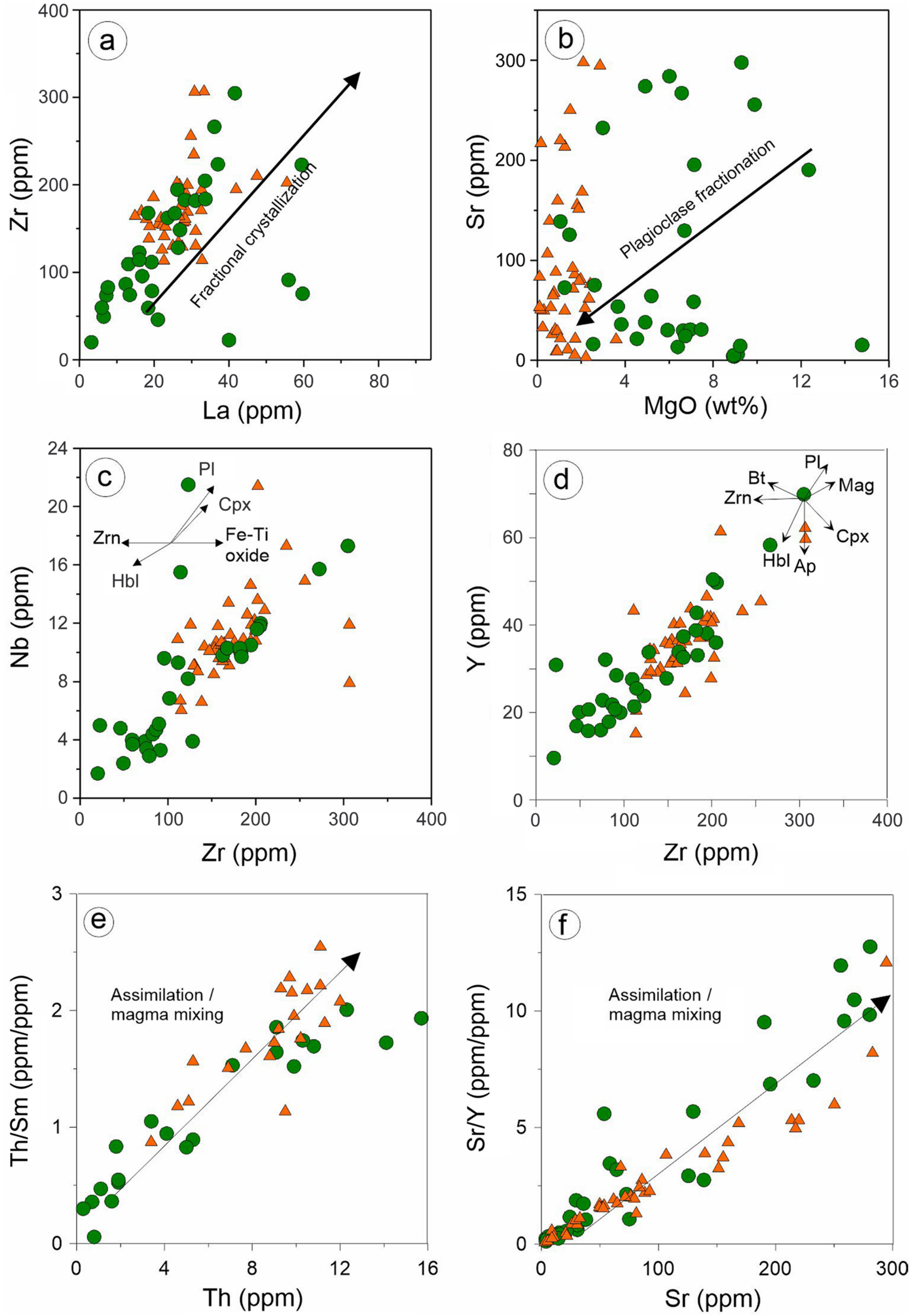

Fig. 9 Plots visualising geochemical patterns of the studied metavolcanic rocks. (**a**) Zr versus La. (**b**) Sr versus MgO. (**c**) Nb versus Zr. (**d**) Y versus Zr. (**e**) Th/Sm versus Th. Sr/Y versus Sr. The mineral differentiation vectors in (**c**) and (**d**) are based on Pearce and Norry (1979). *Ap* apatite, *Bt* biotite, *Cpx* clinopyroxene, *Hbl* hornblende, *Mag* magnetite, *Pl* plagioclase, *Zrn* zircon. Symbols as in Fig. 5

tectonic domains, where they were variably affected by subduction-related metamorphism, arc magmatism, accretionary processes, and post-collisional magmatic activity during the Mesozoic–Cenozoic evolution of the Tethyan realm (Okay et al. 2006; Robertson and Ustaömer 2012). Triassic magmatic activity has been documented in several regions of southern Anatolia, particularly within the ATB (Perinçek 1980; Göncüoğlu et al. 2007; Akal et al. 2007, 2012; Maury et al. 2008; Varol et al. 2011; Özdamar et al. 2013, 2018; and references therein). These volcanic sequences were emplaced within a rift basin that evolved along the northern margin of Gondwana (Göncüoğlu et al. 2007; Akal et al. 2012; Özdamar et al. 2013).

Earlier studies have documented the presence of Middle Carboniferous-Triassic metavolcanic rocks within the Afyon Zone (Kaya et al. 1995; Kurt 1996; Kurt and Arslan 1999; Robertson and Ustaömer 2009; Akal et al. 2011; Candan et al. 2016). These units were initially interpreted

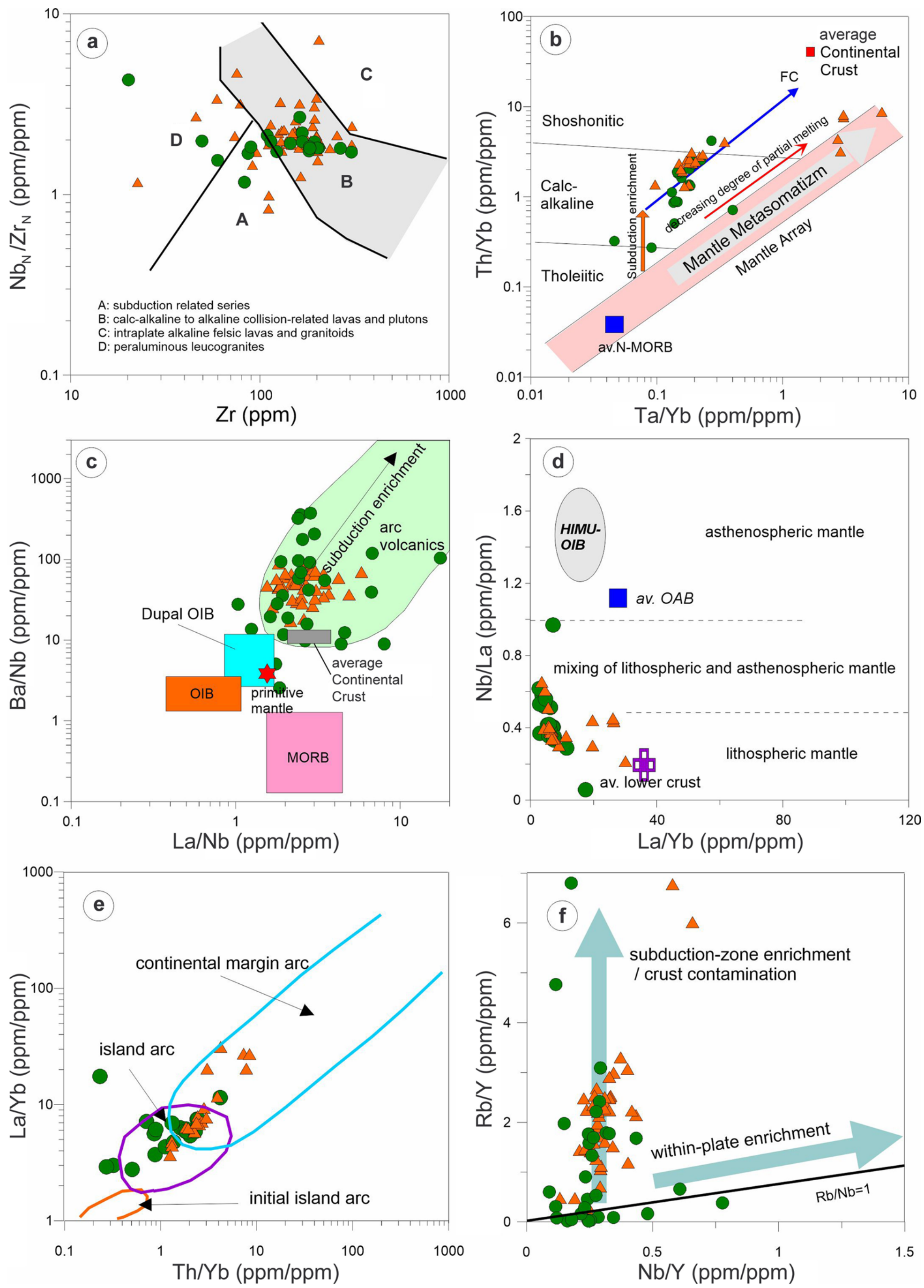

Fig. 10 (**a**) Plot of Nb_N/Zr_N versus Zr in metavolcanic rocks (after Thieblemont and Tegyey 1994); (**b**) Th/Yb versus Ta/Yb (after Pearce et al. 1990); (**c**) Ba/Nb versus La/Nb (after Jahn et al. 1999); (**d**) Nb/La versus La/Yb (after Jahn et al. 1999); (**e**) La/Yb versus Th/Yb and (**f**) Rb/Y versus Nb/Y diagrams. *AFC* assimilation fractional crystallization, *FC* fractional crystallization, *MORB* mid-ocean ridge basalt, *OAB* oceanic island basalt, *PM* primary mantle. Symbols as in Fig. 5

as mid-ocean ridge basalt or products of continental rift volcanism (Kurt and Arslan 1999). However, subsequent radiometric analyses established their Triassic ages: metarhyolites from Düğüncüler (Simav) yielded 240–243 Ma, those from Avdan (Konya) gave 229−224 Ma, and metatrachyandesites from Sızma (Konya) produced 250.1 ± 3.8 Ma (Akal et al. 2011). The metadacite age of 233.4 ± 2.1 Ma obtained in this study aligns closely with these previously reported values. Several studies have linked Triassic magmatic activity in Türkiye to the Variscan Orogeny, a widespread Late Paleozoic orogenic event caused by the collision between Laurasia and Gondwana, responsible for extensive metamorphic and magmatic processes across Central Europe. Although Variscan and Cimmerian deformation and metamorphic overprints are not recognized in the ATB, they are well documented in the Pontides (Okay et al. 2001; Ustaömer et al. 2020). Özdamar et al. (2013) suggested that the geochemical and isotopic characteristics of Triassic meta-rhyolitic rocks in the Afyon Zone support their association with the closure of the Paleotethys Ocean and the opening of the northern branch of the Neotethys Ocean (Fig. 11).

The Middle Carboniferous granites of the Afyon Zone offer metamorphic overprinting consistent with the Triassic-Cenozoic cover sequences, suggesting that continental collision and regional metamorphism were not yet active during granite emplacement. The geochemical signatures of these granites also exhibit depletion-related features comparable to those of the Triassic volcanic rocks, suggesting a genetic continuity between Carboniferous plutonism and Triassic volcanism. The southward subduction of the Paleotethys Ocean beneath Gondwana during Carboniferous is thought to have triggered an extensional tectonic regime along the northern Gondwanan margin, ultimately leading to the rifting and separation of the ATB from the Gondwana supercontinent.

The short-lived southward subduction might have been responsible for the initiation of rifting leading to the separation of the ATB from the main trunk of Gondwana. The pre-Triassic basement of the Afyon Zone was intruded by granitic bodies during low-grade Alpine metamorphism. The geochemical characteristics of granitoids, dated to the Early-Middle Carboniferous (331 to 315 Ma, Candan et al. 2016; and 309–311 Ma Aslan et al. 2026), indicate emplacement in an active magmatic arc setting that developed along the northern margin of Gondwana (Candan et al. 2016; Akal et al. 2024; Aslan et al. 2026). The magmatic rocks spanning the Early to Late Triassic display clear geochemical signatures of subduction-modified magma sources, reflecting the southward subduction of the Paleotethyan oceanic lithosphere beneath the ATB. Candan et al. (2016) stated that, an increase in the subduction angle of the oceanic lithosphere, the initiation of block movements along the Gondwanan margin, and the emplacement of S-type granites in the Middle Carboniferous (309 to 325 Ma), followed by the intrusion of dyke/sill rocks (259.9 to 278.1), reflect a phase of intensified tectono-magmatic activity during Carboniferous period (Akal et al. 2024; Aslan et al. 2026). The Gediktepe massive sulfide deposits are interpreted as products of Triassic rifting-related seafloor hydrothermal vents, likely formed during the Early to Middle Triassic (Aslan et al. 2020b). Considering the field observations and drill core samples obtained from exploration activities in the region, massive sulfide mineralization-bearing metabasalts of Triassic age (Re-Os isochron ages from ore; ~234.5 Ma; Aslan et al. 2020b) are observed as lens-shaped bodies within metadacitic rocks, and metaconglomerates are observed at their base. Therefore, the metabasalts represent the earliest volcanic products formed in the region (Fig. 11). In accordance with the interpretations of Göncüoğlu et al. (2007) and Akal et al. (2012), our newly reported geochemical data indicate that the Triassic facilitated widespread bimodal dacitic and basaltic volcanism correspond to subduction-related magmatic derivatives, whose primary mantle source was substantially modified through metasomatic enrichment and assimilation of crustal components. The integrated geochemical evidence corroborates the inference that these metamorphosed dacitic and basaltic assemblages were emplaced within a rift regime (within-plate tectonic setting) in north Gondwana (Fig. 11).

Finally, northward subduction of the Paleo-Tethyan oceanic lithosphere beneath the southern margin of Laurasia

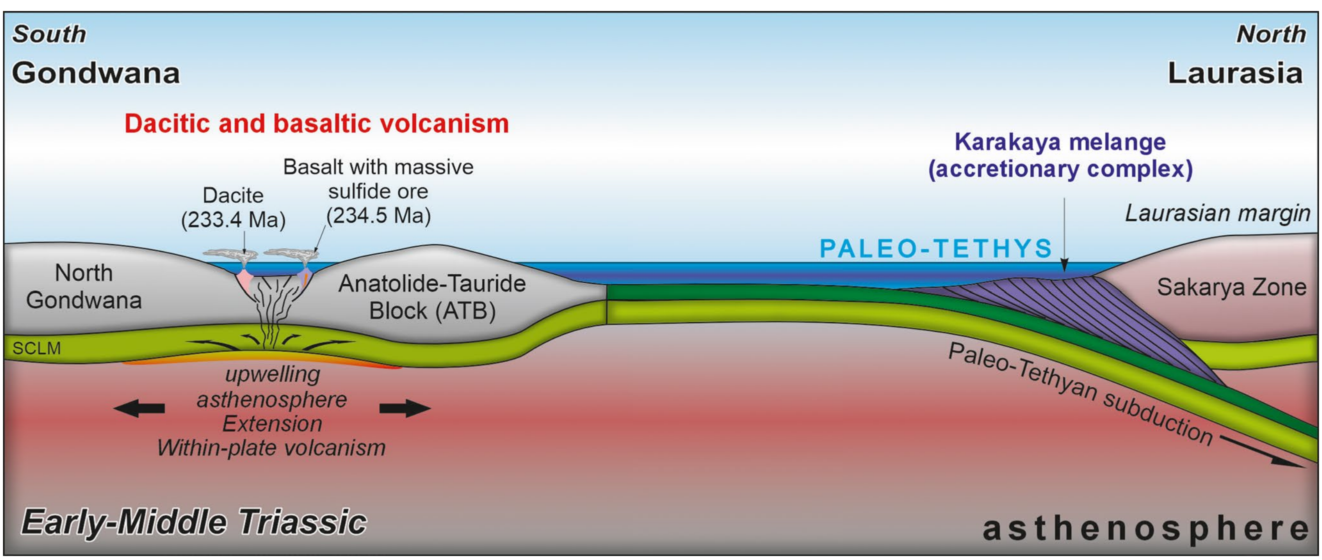

Fig. 11 Schematic model illustrating the tectono-magmatic evolution of the rift-related bimodal metavolcanic rocks of the Afyon Zone in the eastern Mediterranean region during Early-Middle Triassic (modified after; Okay et al. 2002; Akal et al. 2011, 2012, 2024; Okay and Nikishin 2015; Candan et al. 2016). Generation of acidic magmas at ca. 233.4 Ma and basic magmas at ca. 234.5 Ma, forming massif sulfide mineralization, interpreted as products of crustal thinning and asthenospheric upwelling bimodal magmatism

during the Triassic is interpreted to have induced a regional extensional tectonic regime along the northern margin of Gondwana (Fig. 11). Hence, Triassic magmatism documented in the Afyon Zone, together with coeval magmatic activity observed in several tectonic domains of the Anatolides and locally within the Tauride belt, is most plausibly attributed to lithospheric extension and associated mantle melting processes linked to this extensional setting.

Conclusions

Stratigraphically, the northern margin of Gondwana experienced extensional deformation and deep erosion during the Early Triassic (Akal et al. 2024). Within the study area, the metaconglomerates unconformably overlie the Afyon Zone basement rocks and are, in turn, overlain by metabasic volcanic units that locally host massive sulfide mineralization. Geochronological data indicate that the metadacitic rocks crystallized at 233.4 ± 2.1 Ma, based on U–Pb zircon dating, suggesting contemporaneous Late Triassic volcanic activity. Geochemically, the metavolcanic rocks exhibit high-K shoshonitic to calc-alkaline affinities, and trace element patterns show enrichment in LILE (Rb, Ba, Th, U) and depletion in HFSE (Nb, Ti). The enrichment in Th and other incompatible elements reflects a crustal influence during magma evolution. The enrichment of LFSE relative to HFSE, together with $(La/Lu)_N$ values averaging between 10 and 25, is characteristic of calc-alkaline magmatism. Petrogenetically, the metavolcanic rocks evolved through fractional crystallization and assimilation (AFC) processes, with plagioclase and amphibole playing major roles in crystal fractionation. The geochemical signatures suggest that assimilation and/or crustal contamination affected the magmas and that they were generated in an island-arc setting, displaying affinities to T-type MORB. Triassic metavolcanic rocks may be products of magmatic activity belonging to the early stages of the Paleotethys Ocean, which closed by subducting Gondwana to the south, and the Neotethys Ocean, which opened along the northern margin of Gondwana.

Supplementary Information The online version contains supplementary material available at https://doi.org/10.1007/s00710-026-00998-6.

Acknowledgements The authors express their sincere gratitude to Bin Chen for his assistance with the geochronological and isotopic analyses, to Onur Özgür, Cüneyt Bircan and Murat Öntaç for their valuable help during fieldwork, and to Ersin Koralay for his scientific contributions. Major element, trace-element and REE analyses were conducted at the YEBİM Laboratory (Earth Sciences Application and Research Center, Ankara University, Türkiye) and at Acme Analytical Laboratories (Vancouver, Canada). The selection, preparation, CL imaging and U-Pb dating of zircon crystals, as well as Sr and Nd isotopic analyses, were performed at the SHRIMP laboratory of Peking University, PR China. The authors thank two anonymous reviewers and Associate Editor Mohssen Moazzen for their constructive comments and suggestions, which greatly improved the quality of this manuscript. The present study is a part of project 116Y238 supported by the Environment, Atmosphere, Earth and Marine Sciences Research Group (ÇAYDAG) of the Scientific and Technological Research Council of Türkiye (TÜBİTAK).

Author contributions Zafer Aslan: Writing of the article, particularly in the areas of mineralogy-petrography and petrology, figure preparation. Özcan Yiğit: Study of mineralization in metabasalt. M.Selman Aydoğan: Study of mineralization in metabasalt, figure preparation. Yusuf Kağan: Petrology and mineral chemistry studies. All authors reviewed the manuscript.

Data availability No datasets were generated or analysed during the current study.

Declarations

Competing interests The authors declare no competing interests.

References

Akal C, Candan O, Koralay OE, Oberhansli R, Chen F (2005) Metavolcanic rocks in Afyon Zone: implications for Triassic rifting of Neo-Tethyan ocean on Gondwanaland. In: International symposium on the geodynamics of eastern Mediterranean: active tectonics of the Aegean, p 77

Akal C, Candan O, Koralay OE, Chen F, Oberhänsli R (2007) Geochemistry, geochronology and tectonic setting of early Triassic metavolcanics of the Afyon Zone, Turkey. Unpublished TUBITAK Project Report 103Y011, Ankara, Türkiye

Akal C, Candan O, Koralay OE, Okay A, Chen F, Oberhansli R (2011) Afyon Zonu'ndaki (Simav Kuzeyi) Karbonifer Yaşlı Granitlerin Jeolojisi, Jeokimyası ve Jeokronolojisi. TUBITAK Project Report 103Y144, 114 pp, Ankara, Türkiye

Akal C, Candan O, Koralay OE, Oberhänsli R, Chen F, Prelević D (2012) Early Triassic potassic volcanism in the Afyon Zone of the Anatolides/Turkey: implications for the rifting of the Neo-Tethys. Int J Earth Sci 101(1):177–194

Akal C, Candan O, Koralay OE, Gerdes A, Oberhaensli R (2024) Middle triassic magmatism in the Afyon Zone of the Anatolides/Eastern Mediterranean: Implications for the extension of the Northern margin of Gondwana and opening of the Inner-Tauride Ocean. Lithos 482–483:107691

Akdeniz N, Konak N (1979a) Geology of Simav-Emet-Tavşanlı-Dursunbey-Demirci area. Report of the Mineral Research and Exploration Institute, 108 (in Turkish with an abstract in English)

Akdeniz N, Konak N (1979b) Rock units of the Menderes Massif and setting of the metabasic and metaultramafic rocks around Simav. Bull Geol Soc Turkey 22:175–184

Altunkaynak Ş, Dilek Y, Genç ŞC, Sunal G, Gertisser R, Furnes H, Foland KA, Yang J (2012) Spatial, temporal and geochemical evolution of Oligo–Miocene granitoid magmatism in western Anatolia, Turkey. Gondwana Res 21:961–986

Anders B, Reischmann T, Kostopoulos D (2006) Zircon geochronology of pre-Alpine basement rocks, Greece. Int J Earth Sci (Geol Rundsch) 96:639–661

Aslan Z, Erdem D, Temizel İ, Arslan M (2017) SHRIMP U–Pb zircon ages and whole-rock geochemistry for the Şapçı volcanic rocks, Biga Peninsula, Northwest Turkey: implications for pre-eruption crystallization conditions and source characteristics. Int Geol Rev 59(14):1764–1785

Aslan Z, Demir H, Altın İ (2020a) U–Pb zircon geochronology and petrology of the early Miocene Göloba and Şaroluk plutons in the Biga Peninsula, NW Turkey: implications forpost-collisional magmatism and geodynamic evolution. J Afr Earth Sci 172:103998

Aslan Z, Kadıoğlu YK, Yiğit Ö, Aydoğan MS (2020b) Hacıömerderesi (Bigadiç, Balıkesir) civarındaki metamorfik kayaçların petrolojisi ve ilişkili sülfid yatağının kökeni. Unpublished TUBITAK Project Report 106Y238, 230 pp, Ankara, Türkiye

Aslan Z, Kadıoğlu YK, Yiğit Ö, Aydoğan MS (2026) U-Pb zircon geochronology, Sr-Nd isotope geochemistry and petrology of Carboniferous granitic rocks in Afyon Zone (NW Türkiye). J Afr Earth Sci 235:105953

Aydoğan MS (2021) An example of ridge-proximal hydrothermal mineralisation: evidence from radiolarian chert-hosted Fe-Mn-oxide mineralisation within the İzmir-Ankara-Erzincan Neotethyan Ocean, Central Turkey. All Earth 33(1):136–160

Belousova EA, Griffin WL, O'Reilly SY, Fisher NI (2002) Igneous zircon: trace element composition as an indicator of source rock type. Contrib Mineral Petrol 143:602–622

Black LP, Kamo SL, Allen CM, Aleinikoff JK, Davis DW, Korsch RJ, Foudoulis C (2003a) TEMORA 1: a new zircon standard for Phanerozoic U–Pb geochronology. Chem Geol 200:155–170

Black LP, Kamo SL, Williams IS, Mundil R, Davis DW, Korsch RS, Foudoulis C (2003b) The application of SHRIMP to Phanerozoic geochronology; a critical appraisal of four zircon standards. Chem Geol 200:171–188

Bradshaw TK, Smith EI (1994) Polygenetic Quaternary volcanism at Crater Flat, Nevada. J Volcanol Geotherm Res 63:165–182

Candan O, Çetinkaplan M, Oberhansli R, Rimmele G, Akal C (2005) Alpine high-P/low-T metamorphism of the Afyon Zone and implications for the metamorphic evolution of Western Anatolia, Turkey. Lithos 84:102–124

Candan O, Akal C, Koralay OE, Okay AI, Oberhänsli R, Prelević D, Mertz-Kraus R (2016) Carboniferous granites on the northern margin of Gondwana, Anatolide-Tauride Block, Turkey – evidence for southward subduction of Paleotethys. Tectonophysics 683:349–366

Çelik ÖF, Marzoli A, Marschik R, Chiaradia M, Neubauer F, Öz İ (2011) Early-Middle Jurassic intra-oceanic subduction in the İzmir-Ankara-Erzincan Ocean, Northern Turkey. Tectonophysics 509(1–2):120–134

Cocks LRM, Torsvik TH (2002) Earth geography from 500 to 400 million years ago: a faunal and palaeomagnetic review. J Geol Soc Lond 159:631–644

Dannat C, Reischmann T (1998) Geochronological, geochemical and isotopic data on granitic gneisses from the Menderes Massif, SW Turkey. 3rd International Turkish Geology Symposium, Ankara, Abstracts, p 275

Dilek Y, Moores EM (1990) Regional Tectonics of the Eastern Mediterranean ophiolites. In: Malpas J, Moores EM, Panayiotou A, Xenophontos C (eds) Ophiolites, Oceanic Crustal Analogues. Proceedings of the Symposium, Troodos, pp 295–309

Dilek Y, Thy P (2006) Age and petrogenesis of plagiogranite intrusions in the Ankara melange, Central Turkey. Island 15(1):44–57

Domeier M, Torsvik TH (2014) Plate tectonics in the late Paleozoic. Geosci Front 5(3):303–350

Elburg MA, Bergen MV, Hoogewerff J, Foden J, Vroon P, Zulkarnain I, Nasution A (2002) Geochemical trends across an arc-continent collision zone: magma sources and slab-wedge transfer processes below the Pantar Strait volcanoes, Indonesia. Geochim Cosmochim Acta 66:2771–2789

Faure G (2001) Origin of Igneous Rocks: The Isotopic Evidence. Springer-Verlag, Heidelberg, Germany, p 496

Gill JB (1981) Orogenic Andesites and Plate Tectonics. Springer, Berlin, p 390

Göncüoğlu MC, Özcan A, Turhan N, Işık A (1997) Distribution of Lower Paleozoic Units in the Alpine Terranes of Turkey: paleogeographic constraints. In: Göncüoğlu MC, Derman AS (eds) Lower Palaezoic Evolution in northwest Gondwana, vol 3. Turk Assoc Petr Geol Special Publication, pp 13–24

Göncüoğlu MC, Yalınız MK, Tekin UK (2006) Geochemistry, tectonomagmatic discrimination and radiolarian ages of basic extrusives within the Izmir-Ankara suture belt (NW Turkey): time constraints for the Neotethyan evolution. Ofioliti 31:25–38

Göncüoğlu MC, Çapkınoğlu Ş, Gürsu S, Noble P, Turhan N, Tekin UK, Okuyucu C, Göncüoğlu Y (2007) The Mississippian in the Central and Eastern Taurides (Turkey): constraints on the tectonic setting of the Tauride-Anatolide platform. Geol Carpath 58:427–442

Göncüöğlu MC, Turhan N, Tekin K (2003) Evidence for the Triassic rifting and opening of the Neotethyan Izmir-Ankara ocean, northern edge of the Tauride-Anatolide platform, Turkey. Bull Geol Soc Italy Spec Vol 2:203–212

Güngör T, İşintek İ, Akay E, Akal C, Hasözbek A, Erbil A, Gerdes A (2025) Kinematics and age of the Afyon Zone in the Akhisar region, western Türkiye. Turk J Earth Sci 34:23–46

Hart SR, Gerlach DC, White WM (1986) A possible new Sr-Nd-Pb mantle array and consequences for mantle mixing. Geochim Cosmochim Acta 50:1551–1557

Hetzel R, Reischmann T (1996) Intrusion age of Pan-African augen gneisses in the southern Menderes massif and the age of cooling after Alpine ductile extensional deformation. Geol Mag 133:565–572. https://doi.org/10.1080/10739140903252956

Irvine TN, Baragar WRA (1971) A guide to the chemical classification of common volcanic rocks. Can J Earth Sci 8:523–548

Jacobsen SB, Wasserburg GJ (1980) Sm-Nd isotopic evolution of chondrites. Earth Planet Sci Lett 50:139–155

Jahn BM, Wu F, Lo CH, Tsai CH (1999) Crust-mantle interaction induced by deepsubduction of the continental crust: geochemical and Sr-Nd isotopic evidence frompost-collisional maficultramafic intrusions of the northern Dabie complex, central China. Chem Geol 157:119–146

Kadıoğlu YK, Dilek Y, Foland KA (2006) Slab break-off and syncollisional origin of the Late Cretaceous magmatism in the Central Anatolian crystalline complex, Turkey. In: Yıldırım D, Sypros P (eds) Postcollisional Tectonics and Magmatism in the Mediterranean Region and Asia. Geol Soc Am Spec Pap 409, pp 381–415

Kadıoğlu YK, Üstündağ Z, Deniz K, Yenikaya C, Erdoğan Y (2009) XRF and Raman characterization of antimonite. Instrum Sci Technol 37:683–696. https://doi.org/10.1080/10739140903252956

Kaya O, Sadeddin W, Altıner D, Meriç E, Tansel İ, Vural A (1995) Tavşanlı (Kütahya) güneyindeki ankimetamorfik kayaların stratigrafisi ve yapısal konumu: İzmir Ankara Zonu ile bağlantısı. Bull Min Res Exp 117:5–16

Kirkland CL, Smithies RH, Taylor RJM, Evans N, McDonald B (2015) Zircon Th/U ratios in magmatic environs. Lithos 212–215:397–414

Koralay OE, Satır M, Dora O (2001) Geochemical and geochronological evidence for early Triassic calc-alkaline magmatism in the Menderes Massif, western Turkey. Int J Earth Sci 89:822–835

Kurt H (1996) Geochemical characteristics of the meta-igneous rocks near Kadınhanı (Konya), Turkey. Geosound 28:1–22

Kurt H, Arslan M (1999) Kadınhanı (Konya) K'ca zengin metatrakiandezitinin jeokimyası ve petrojenezi: Devoniyen(?) volkanizmasının gelişimi. Geol Bull Turk 42(1):57–67

Le Maitre RW, Streckeisen A, Zanettin B, Le Bas MJ, Bonin B, Bateman P, Bellieni G, Dudek A, Efremova S, Keller J, Lamere J, Sabine PA, Schmid R, Sorensen H, Woolley AR (2002) Igneous rocks: A classification and glossary of terms. Recommendations of the International Union of Geological Sciences Subcommission on the Systematics of Igneous Rocks, 2nd edn. Cambridge University Press, Cambridge, UK

Li CF, Li XH, Li QL, Guo JH, Yang YH (2012) Rapid and precise determination of Sr and Nd isotopic ratios in geological samples from the same filament loading by thermal ionization mass spectrometry employing a single-step separation scheme. Anal Chim Acta 727(10):54–60

Ludwig KR (2003) ISOPLOT 3.0: A geochronological toolkit for microsoft excel. Berkeley Geochronology Center. Special Publication 4

Maury RC, Lapierre H, Bosch D, Marcoux J, Krystyn L, Cotten J, Bussy F, Brunet P, Sénebier F (2008) The alkaline intraplate volcanism of the Antalya Nappes (Turkey): a Late Triassic remnant of the Neotethys. Bull Soc Geol Fr 179:397–410

Middlemost EAK (1994) Naming materials in the magma/igneous rock system. Earth Sci Rev 37:215–224

Miyashiro A (1978) Nature of alkalic volcanic rock series. Contrib Mineral Petrol 66:91–104

Moix P, Beccaletto L, Kozur HW, Hochard C, Rosselet F, Stampfli GM (2008) A new classification of the Turkish terranes and sutures and its implication for the paleotectonic history of the region. Tectonophysics 451:7–39

Moix P, Beccaletto L, Masset O, Kozur HW, Dumitrică P, Vachard D, Martini R, Stampfli GM (2011) Geology and correlation of the Mersin Mélanges, Southern Turkey. Turk J Earth Sci 20:57–98

Mposkos E, Krohe A (2004) New evidences of the low-P/high-T pre-Alpine metamorphism and medium-P Alpine overprint of the Pelagonian zone documented in metapelites and orthogneisses from the Voras Massif, Macedonia, northern Greece. Bull Geol Soc Greece 26:558–567

Okay AI (1984) Distribution and characteristics of the Northwest Turkey blueschists. In: Robertson AHF, Dixon JA (eds) The Geological Evolution of the Eastern Mediterranean, Geol Soc London Spec Publ 17, pp 455–466

Okay AI, Nikishin AM (2015) Tectonic evolution of the southern margin of Laurasia in the Black Sea region. Int Geol Rev 57:1051–1076

Okay AI, Tüysüz O (1999) Tethyan sutures of Northern Turkey. In: Durand B, Jolivet L, Horthváth F, Séranne M (eds) The Mediterranean Basin: Tertiary Extension within the Alpine Orogen. Geol Soc London Spec Publ 156, pp 475–515

Okay AI, Satır M, Maluski H, Siyako M, Monie P, Metzger R, Akyüz S (1996) Palea- and Neo-Tethyan events in northwestern Turkey: Geologic and geochronologic constraints. In: Yın A, Harrison M (eds) Tectonic of Asia. Cambridge University Press, pp 420–441

Okay AI, Harris N, Kelley S (1998) Exhumation of blueschists along a Tethyan suture in northwest Turkey. Tectonophysics 285:275–299

Okay AI, Satır M, Tüysüz O, Akyüz S, Chen F (2001) The tectonics of the Strandja Massif: late-Variscan and mid-Mesozoic deformation and metamorphism in the northern Aegean. Int J Earth Sci 90:217–233

Okay AI, Monod O, Monié P (2002) Triassic blueschists and eclogites from northwest Turkey: vestiges of the Paleo-Tethyan subduction. Lithos 64:155–178

Okay AI, Satır M, Siebel W (2006) Pre-Alpide Paleozoic and Mesozoic orogenic events in the Eastern Mediterranean region. In: Igee DG, Stephenson RA (eds) European Lithosphere Dynamics. Geol Soc Lond Mem 32:389–405

Özcan A, Göncüoğlu MC, Turhan N, Uysal S, Şentürk K (1988) Late Paleozoic evolution of the Kütahya–Bolkardağ Belt. J Pure Appl Sci 21:211–220

Özdamar Ş, Billor MZ, Sunal G, Esenli F, Roden MF (2013) First U–Pb SHRIMP zircon and $^{40}Ar/^{39}Ar$ ages of metarhyolites from the Afyon–Bolkardag Zone, SW Turkey: implications for the rifting and closure of the Neo-Tethys. Gondwana Res 24:377–391

Özdamar Ş, Sunal G, Demiroğlu M, Yaltırak C, Billor MZ, Georgiev S, Hames W, Dunkl I, Aydin HC (2018) Metamorphism, magmatism, and exhumation history of the Tavşanlı Zone, NW Turkey: new petrological constraints. Turk J Earth Sci 27(4):269–293

Pearce JA, Norry MJ (1979) Petrogenetic implications of Ti, Zr, Y and Nb variations in volcanic rocks. Contrib Mineral Petrol 69:33–47

Pearce JA, Bender JF, De Long SE, Kidd WSF, Low PJ, Güner Y, Şaroğlu F, Yılmaz Y, Moorbath S, Mitchell JJ (1990) Genesis of collision volcanism in eastern Anatolia Turkey. J Volcanol Geotherm Res 44:189–229

Pehlivan S, Duru M, Dönmez M, Ilgar A, Akçay AE, Erdoğan K, Özer D (2007) 1/100.000 ölçekli Türkiye Jeoloji haritaları, Balıkesir I 19 paftası. Min Res Exp 96(40), Ankara

Perinçek D (1980) Bitlis metamorfitlerinde volkanitli Triyas. Geol Bull Turk 19:65–78 (in Turkish with English abstract)

Pourteau A, Sudo M, Candan O, Lanari P, Vidal O, Oberhansli R (2013) Neotethys closure history of Anatolia: insights from ^{40}Ar–^{39}Argeochronology and P–Testimation in high-pressuremetasedimentary rocks. J Metamorph Geol 31:585–606

Pupin JP (1980) Zircon and granite petrology. Contrib Mineral Petrol 73:207–220

Reischmann T, Kostopoulos DK, Loos S, Anders B, Avgerinas A, Sklavounos SA (2001) Late Paleozoic magmatism in the basement rocks southwest of the Mt. Olympos, Central Pelagonian Zone, Greece: remnants of a Permo-Carboniferous magmatic arc. Bull Geol Soc Greece 25:985–993

Robertson AHF, Dixon JE (1984) Introduction: aspects of the geological evolution of the eastern Mediterranean. In: Dixon JE, Robertson AHF (eds) The Geological Evolution of the Eastern Mediterranean. Geol Soc London Spec Publ 17, pp 1–74

Robertson AHF, Ustaömer T (2009) Upper Palaeozoic subduction/accretion processes in the closure of Palaeotethys: evidence from the Chios Melange (E Greece), the Karaburun Melange (W Turkey) and the Teke Dere Unit (SW Turkey). Sediment Geol 220:29–59

Robertson AHF, Ustaömer T (2012) Testing alternative tectono-stratigraphic interpretations of the Late Palaeozoic-Early Mesozoic Karakaya complex in NW Turkey: support for an accretionary origin related to northward subduction of Palaeotethys. Turk J Earth Sci 21:961–1007

Şengör AMC (1979) Mid-mesozoic closure of Permo-Triassic Tethys and its implications. Nat 279:590–593

Şengör AMC, Yılmaz Y (1981) Tethyan evolution of Turkey: a plate tectonic approach. Tectonophysics 75:181–141

Şengör AMC, Satır M, Akkök R (1984) Timing of tectonic events in the Menderes Massif, Western Turkey: implications for tectonic evolution and evidence for Pan-African bassement in Turkey. Tectonics 3(7):693–707

Sherlock S, Kelley SP, Inger S, Harris N, Okay AI (1999) ^{40}Ar-^{39}Ar and Rb-Sr geochronology of high-pressure metamorphism and exhumation history of the Tavşanlı Zone, NW Turkey. Contrib Mineral Petrol 137:46–58

Smith EI, Sanchez A, Walker JD, Wang K (1999) Geochemistry of mafic magmas in the Hurricane Volcanic field, Utah: implications for small- and large-scale chemical variability of the lithospheric mantle. J Geol 107:433–448

Stampfli GM, Borel GD (2002) A plate tectonic model for the Palaeozoic and Mesozoic constrained by dynamic plate boundaries and restored synthetic oceanic isochrons. Earth Planet Sci Lett 19:17–33

Stampfli G, Vavassis I, Bono A, De, Rosselet F, Matti B, Bellini M (2003) Remnants of the Paleotethys oceanic suture-zone in the western Tethyan area. In: Cassinis G, Decandia FA (eds) Stratigraphic and Structural Evolutionon the Late Carboniferous to

Triassic Continental and Marine Successions in Tuscany (Italy): Regional Reports and General Correlation. Bull Soc Geol Ital 2 pp 1–23

Sun S, McDonough WF (1989) Chemical and isotopic systematics of oceanic basalt: Implications for mantle composition and processes. In: Saunders AD, Norry MJ (eds) Magmatism in the Ocean Basins. Geol Soc Lond Spec Publ 42 pp 313–345

Thieblemont D, Tegyey Y (1994) Geochemical discrimination of differentiated magmaticrocks attesting for the variable origin and tectonic setting of calc-alkalinemagmas. C R Acad Sci Ser IIA 319:87–94

Thirlwall MF (1991) Long-term reproducibility of multicollector Sr and Nd isotope ratio analysis. Chem Geol 94(2):85–104

Thirlwall MF, Smith TE, Graham AM, Theodorou N, Hollings P, Davidson JP, Arculus RJ (1994) High field strength element anomalies in arc lavas; source or process? J Petrol 35:819–838

Thompson RN, Morrison MA, Hendry GL, Parry SJ (1984) An assessment of the relative roles of crust and mantle in magma genesis: an elemental approach. Philos Trans A Math Phys Eng Sci (1984) 310 (1514): 549–590

Ustaömer T, Ustaömer PA, Robertson AHF, Gerdes A (2020) U-Pb-Hf isotopic data from detrital zircons in late Carboniferous and Mid-Late Triassic sandstones, and also Carboniferous granites from the Tauride and Anatolide continental units in S Turkey: implications for Tethyan palaeogeography. Int Geol Rev 62(9):1159–1186

Varol E, Bedi Y, Tekin UK, Uzunçimen S (2011) Geochemical and petrological characteristics of Late Triassic basic volcanic rocks from the Kocalı Complex, SE Turkey: implications for the Triassic evolution of southern Tethys. Ofioliti 36(1):101–115

White WM, Patchett J (1984) Hf–Nd–Sr isotopes and incompatible element abundances in island arcs: implications for magma origins and crust-mantle evolution. Earth Planet Sci Lett 67:167–185

Winchester JA, Floyd PA (1977) Geochemical discrimination of different magma series and their differentiation products using immobile elements. Chem Geol 20:325–343

Zindler A, Hart SR (1986) Chemical geodynamics. Annu Rev Earth Planet Sci 14:493–571

Zlatkin O, Avigad D, Gerdes A (2017) The Pelagonian terrane of Greece in the peri-Gondwanan mosaic of the Eastern Mediterranean: implications for the geological evolution of Avalonia. Precambrian Res 290:163–183